Bioactive Materials 27 (2023) 409–428

Contents lists available at ScienceDirect

Bioactive Materials

journal homepage: www.keaipublishing.com/en/journals/bioactive-materials

Double-network hydrogel enhanced by SS31-loaded mesoporous polydopamine nanoparticles: Symphonic collaboration of near-infrared photothermal antibacterial effect and mitochondrial maintenance for full-thickness wound healing in diabetes mellitus

Qing-Song Deng [a,b,c,1], Yuan Gao [a,b,c,1], Bi-Yu Rui [a,b,1], Xu-Ran Li [a,b,c], Po-Lin Liu [a,b,c], Zi-Yin Han [d], Zhan-Ying Wei [e], Chang-Ru Zhang [f,g], Fei Wang [h], Helen Dawes [i,j,k], Tong-He Zhu [l], Shi-Cong Tao [a,b,*], Shang-Chun Guo [a,b,c,**]

[a] Department of Orthopedic Surgery, Shanghai Sixth People's Hospital Affiliated to Shanghai Jiao Tong University School of Medicine, 600 Yishan Road, Shanghai, 200233, China
[b] School of Medicine, Shanghai Jiao Tong University, 227 South Chongqing Road, Shanghai, 200025, China
[c] Institute of Microsurgery on Extremities, Shanghai Sixth People's Hospital Affiliated to Shanghai Jiao Tong University School of Medicine, 600 Yishan Road, Shanghai, 200233, China
[d] Department of Rheumatology, The Affiliated Changzhou No. 2 People's Hospital of Nanjing Medical University, No.29, Xinglongxiang, Tianning District, Changzhou, 213000, China
[e] Shanghai Clinical Research Centre of Bone Diseases, Department of Osteoporosis and Bone Diseases, Shanghai Sixth People's Hospital Affiliated to Shanghai Jiao Tong University School of Medicine, Shanghai, 200233, China
[f] Shanghai Key Laboratory of Orthopedic Implants, Department of Orthopedic Surgery, Shanghai Ninth People's Hospital, Shanghai Jiao Tong University School of Medicine, No. 639 Zhizaoju Road, Shanghai, 200011, China
[g] Clinical and Translational Research Center for 3D Printing Technology, Medical 3D Printing Innovation Research Center, Shanghai Ninth People's Hospital, Shanghai Jiao Tong University School of Medicine, Shanghai, 200125, China
[h] Department of Orthopedics, Shanghai Key Laboratory for Prevention and Treatment of Bone and Joint Diseases, Shanghai Institute of Traumatology and Orthopedics, Ruijin Hospital, Shanghai Jiao Tong University School of Medicine, 197 Ruijin Second Road, Shanghai, 200025, China
[i] Faculty of Health and Life Science, Oxford Brookes University, Headington Road, Oxford, OX3 0BP, UK
[j] NIHR Oxford Health Biomedical Research Centre, Oxford, OX3 7JX, UK
[k] College of Medicine and Health, St Lukes Campus, University of Exeter, Heavitree Road, Exeter, EX1 2LU, UK
[l] School of Chemistry and Chemical Engineering, Shanghai Engineering Research Center of Pharmaceutical Intelligent Equipment, Shanghai Frontiers Science Research Center for Druggability of Cardiovascular Non-Coding RNA, Institute for Frontier Medical Technology, Shanghai University of Engineering Science, Shanghai, China

ARTICLE INFO

Keywords:
Mesoporous polydopamine nanoparticles (MPDA NPs)
SS31
Photothermal antibacterial
Mitochondrial function maintenance
Diabetic wound healing

ABSTRACT

Diabetic wound healing has become a serious healthcare challenge. The high-glucose environment leads to persistent bacterial infection and mitochondrial dysfunction, resulting in chronic inflammation, abnormal vascular function, and tissue necrosis. To solve these issues, we developed a double-network hydrogel, constructed with pluronic F127 diacrylate (F127DA) and hyaluronic acid methacrylate (HAMA), and enhanced by SS31-loaded mesoporous polydopamine nanoparticles (MPDA NPs). As components, SS31, a mitochondria-targeted peptide, maintains mitochondrial function, reduces mitochondrial reactive oxygen species (ROS) and thus regulates macrophage polarization, as well as promoting cell proliferation and migration, while MPDA NPs not only scavenge ROS and exert an anti-bacterial effect by photothermal treatment under near-infrared light irradiation, but also control release of SS31 in response to ROS. This F127DA/HAMA–MPDA@SS31 (FH–M@S) hydrogel has characteristics of adhesion, superior biocompatibility and mechanical properties which can adapt to

Peer review under responsibility of KeAi Communications Co., Ltd.
* Corresponding author. Department of Orthopedic Surgery, Shanghai Sixth People's Hospital Affiliated to Shanghai Jiao Tong University School of Medicine, 600 Yishan Road, Shanghai, 200233, China.
** Corresponding author. Department of Orthopedic Surgery, Shanghai Sixth People's Hospital Affiliated to Shanghai Jiao Tong University School of Medicine, 600 Yishan Road, Shanghai, 200233, China.
E-mail addresses: sctao@shsmu.edu.cn (S.-C. Tao), scguo@shsmu.edu.cn (S.-C. Guo).
[1] These authors contributed equally to this work.

https://doi.org/10.1016/j.bioactmat.2023.04.004
Received 20 October 2022; Received in revised form 24 March 2023; Accepted 2 April 2023

irregular wounds at different body sites and provide sustained release of MPDA@SS31 (M@S) NPs. In addition, in a diabetic rat full thickness skin defect model, the FH–M@S hydrogel promoted macrophage M2 polarization, collagen deposition, neovascularization and wound healing. Therefore, the FH–M@S hydrogel exhibits promising therapeutic potential for skin regeneration.

1. Introduction

Diabetic wounds, a typical and severe complication of diabetes, significantly impact patients' quality of life, due to delayed healing, recurrent infection, and even amputation [1,2]. With the morbidity of diabetes increasing annually, a quarter of patients will develop a diabetic foot ulcer, which imposes a major burden on human healthcare and the social economy [3,4]. Although there are a variety of treatment strategies to promote diabetic wound healing, such as delivery of cells or growth factors, surgical debridement, and vascular reconstruction, these therapies are costly and have limited effect [5,6]. However numerous studies have shown that two main factors typical of diabetic wounds-chronic bacterial infection and permeation of the micro-environment by reactive oxygen species (ROS) due to hyperglycemia and mitochondrial dysfunction-cause persistent inflammation, vascular endothelial dysfunction and tissue necrosis [7–10].

Numerous factors increase the level of ROS, for example, activation of the receptor for advanced glycation end products (RAGE), prolonged bacterial infection, and ischemia, but the majority of ROS originate from mitochondria (mtROS) as a result of mitochondrial dysfunction [11]. In a high-glucose environment, as mitochondrial metabolism becomes disordered, cardiolipin is decreased and undergoes peroxidation, and the function of the electron transport chain (ETC) is changed, resulting in attenuation of oxidative phosphorylation (OXPHOS), adenosine triphosphate (ATP) insufficiency, leakage of a large number of mtROS, and eventually dysregulated macrophage polarization, chronic inflammation, and microvascular damage [12–15].

Apart from severe oxidative stress, bacterial infection in the wound is another intractable problem [8,16]. More than half of diabetic ulcer patients will be infected, and approximately 20% will experience amputation attributable to severe infection [17,18]. Furthermore, bacterial infection is one of the major factors in the delayed healing of diabetic wounds, causing persistent inflammation, tissue necrosis, and ultimately necessitating amputation [19]. Although all kinds of antibiotics have been used to treat resistant bacterial infection, chronic administration of antibiotics will lead to drug resistance. In recent years, various biomaterials with superior antibacterial properties have been developed including silver ions, copper ions, and zinc oxide, but these metallic ions can cause serious tissue toxicity [20,21]. Hence, it is extremely urgent to develop a type of biomaterial that can not only act to hinder mtROS generation and enhance energy supplementation during hyperglycemia, but can also sterilize a wound in a biosafe and efficient way.

SS31, a mitochondria-targeted peptide, selectively binds to cardiolipin, a phospholipid, which is exclusively located on the inner mitochondrial membrane [22] and is one of the components crucial to crista formation [23]. SS31 inhibits oxidation of cardiolipin and cytochrome C, and weakens the interaction between them [13,24]. Meanwhile, SS31 stabilizes the electron transport chain, enhancing electron transfer and oxidative phosphorylation [24], reducing the production of mtROS, and increasing the synthesis of ATP [25] via electrostatic and hydrophobic interactions with cardiolipin [26]. With reduced mtROS production and sufficient ATP availability, macrophages are polarized to M2 macrophages and the secretion of many growth factors, such as vascular endothelial growth factor (VEGF) and epidermal growth factor (EGF), will increase, thus enhancing cells' capacities of adhesion, proliferation, and migration [27–30].

As previous studies suggested that SS31 can be applied in the treatment of oxidative-associated diseases [31,32], we attempted to employ SS31 to maintain mitochondrial function and accelerate diabetic wound healing. However, the use of SS31 for therapeutic applications introduces a series of limiting factors to be overcome, because the single cationic bioactive peptide is easily hydrolyzed, rapidly metabolized, unevenly distributed, and quickly lost, leading to low bioavailability and poor therapeutic effect [26,33].

Polydopamine nanoparticles (PDA NPs), self-polymerized by dopamine, a natural neurotransmitter [34], have been widely used for drug delivery because of their biodegradability, good biocompatibility, and excellent photothermal transfer efficiency [34,35]. PDA NPs have abundant reactive catechol/quinone, amine, and imine groups, which can bond with other molecules via interactions including π-π stacking, hydrogen bonding, and electrostatic attraction [36,37]. However, the drug-load capacity of PDA NPs is limited by the available specific surface area [36]. Hence, mesoporous polydopamine nanoparticles (MPDA NPs) are used to enhance the drug-load ratio [38]. In addition, MPDA NPs are a photothermal conversion agent and have striking photothermal conservation capacity, so that they can generate a thermal reaction after exposure to near-infrared irradiation (NIR) [39]. Under illumination with an 808 nm laser, the temperature of MPDA NPs will rapidly increase, and they will function as a sterilizing and anti-biofilm formation agent [40,41]. Furthermore, MPDA NPs possess a large number of phenolic groups which can provide great ROS scavenging ability [42]. As ROS are reduced, the expression of proinflammatory cytokines will also decrease and the process of wound healing will accelerate [43,44].

Hydrogels are widely used in tissue engineering owing to their three-dimensional structure which is similar to that of extracellular matrix (ECM) [45]. Hyaluronic acid (HA) has been considered an excellent dressing or a carrier to deliver drugs and promote wound healing, due to its superior properties including biodegradability, biocompatibility, and high water absorption capacity [46,47]. Adding methacrylate onto the backbone of HA transforms HA into hyaluronic acid methacrylate (HAMA) and confers the ability to photopolymerize. However, an ideal wound dressing possesses not merely good biological properties, but good mechanical properties also play a vital role [48]. Recently, a great deal of attention has been paid to the use of hydrogels in accelerating wound healing but this has neglected the facts that wounds usually occur in certain active body sites, and usually in a particular shape. F127DA, a PEO-PPO-PEO triblock polymer, can self-assemble to generate a hydrogel with excellent mechanical properties and injectability [49]. Compared with single-network hydrogel, the injectable multi-crosslinked double-network hydrogel FH (F127DA and HAMA) retains the remarkable biological properties of HAMA and the mechanical characteristics of F127DA.

In this study, we designed an FH double-crosslinked hydrogel enhanced by MPDA@SS31 nanoparticles (M@S NPs) to promote chronic diabetic wound healing. This hydrogel exhibited excellent biological properties, injectability, adhesion and mechanical properties. These characteristics demonstrated that the FH–M@S (F127DA/HAMA–MPDA@SS31) hydrogel can be used to treat irregular wounds. Furthermore, this hydrogel possesses antibacterial properties due to photothermal conversion of MPDA NPs. Meanwhile, FH hydrogel also provides sustained release of M@S NPs. With the release of MPDA NPs and SS31, the degree of oxidative stress in the wound will be reduced and mitochondrial function will be enhanced, regulating macrophage polarization, alleviating inflammation and constantly inducing revascularization in the wound. In order to prove our hypothesis, the interactions between MPDA NPs and SS31 and their hydrogel properties were investigated. Then the capacities of antibacterial efficiency,

increasing cell viability, ROS scavenging, enhancing angiogenesis, and regulating macrophage polarization were assessed *in vitro*. Finally, the hydrogel was used to treat full-thickness wounds in a diabetic model and the results indicated that the FH–M@S hydrogel accelerates wound closure by regulating macrophage polarization, and enhancing re-epithelialization, collagen deposition and neovascularization.

2. Materials and methods

All methods can be found in the accompanying supplementary materials.

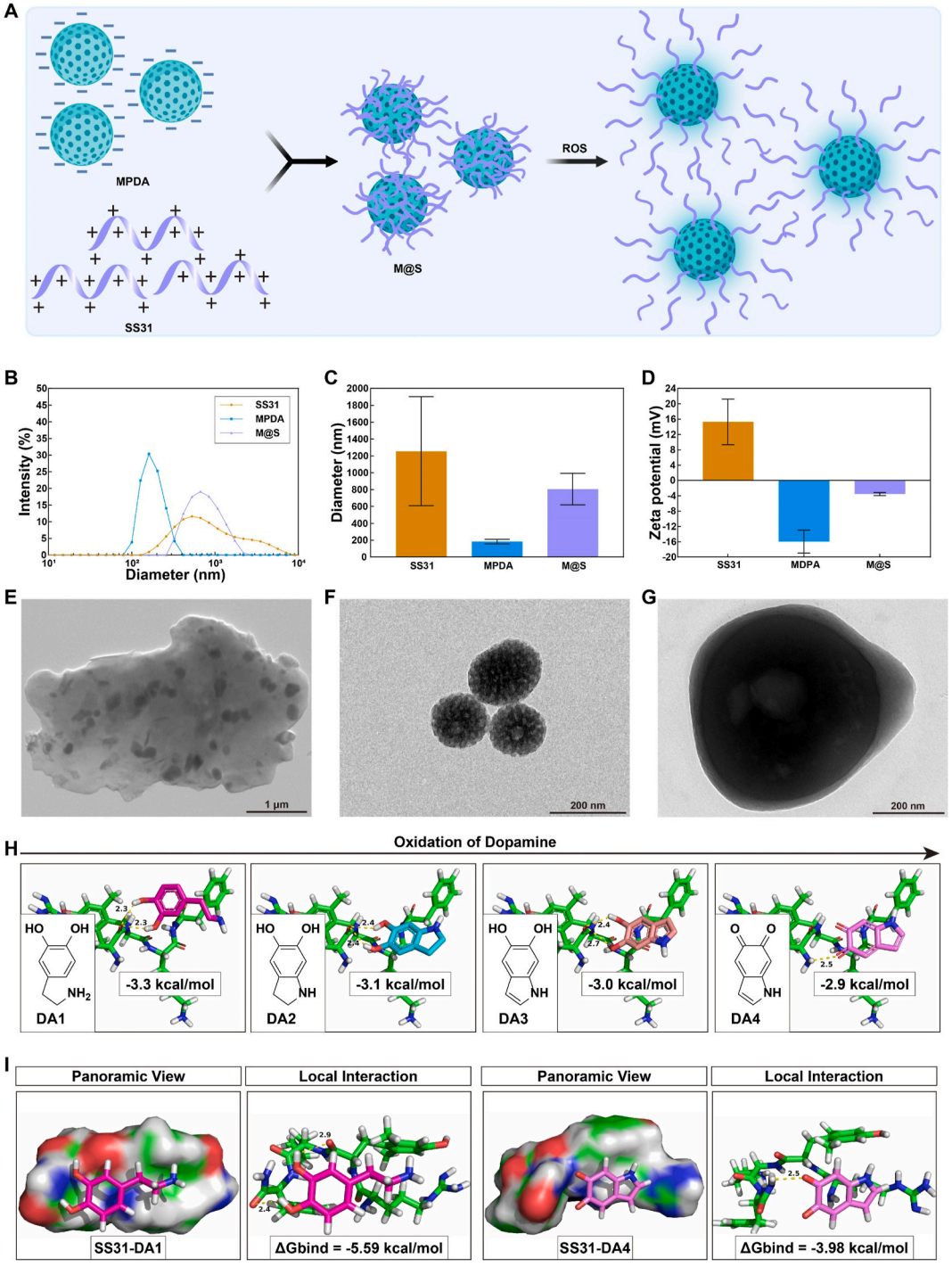

Fig. 1. Characteristics of M@S NPs. (A) Schematic illustration of the synthesis of M@S NPs and release of SS31. This illustration was created with BioRender.com. (B, C) Particle size distribution of SS31, MPDA NPs, and M@S NPs. (D) Zeta potential of SS31, MPDA NPs, and M@S NPs. (E, F, G) TEM images of SS31, MPDA NPs, and M@S NPs. (H) Molecular docking study between SS31 and four different redox states of PDA NPs monomers (DA1, DA2, DA3, and DA4). (I) Molecular dynamics simulation panoramic view and local interaction of SS31–DA1 complex and SS31–DA4 complex.

3. Results and discussion

3.1. Formulation and characterization of SS31-loaded MPDA NPs

As described in previous studies, owing to their large number of phenolic hydroxyl groups, MPDA NPs can adsorb many molecules via electrostatic interaction and hydrogen bonding [36,37]. SS31, a positively-charged peptide with many amidogens [26], was adsorbed onto the MPDA NPs (Fig. 1A). Dynamic light scattering (DLS) was used to analyze the Zeta potential and size distribution of the SS31, MPDA NPs, and M@S NPs (Fig. 1B and C). The results revealed that the size distribution of SS31 was from 161.11 nm to 7209.36 nm and the average size was 1256.00 ± 647.28 nm, which was considerably scattered. To deliver SS31 in a simple and convenient way and accelerate SS31 dispersion, SS31 solution was mixed with a solution of MPDA NPs and incubated for 24 h which generated M@S NPs by electrostatic self-assembly. The average sizes of MPDA NPs and M@S NPs were 182.90 ± 27.01 nm and 806.10 ± 185.78 nm, respectively. As shown in Fig. 1D, the Zeta potential of the SS31 solution was 15.29 ± 5.84 mV, and the MPDA NPs had a negative charge of −15.98 ± 2.94 mV, while the M@S NP solution was near electrically neutral (−3.54 ± 0.39 mV). These data indicated that the SS31 positively-charged particles can attach to the MPDA negatively-charged particles to electrostatically self-assemble. Transmission electron microscopy (TEM) showed that SS31 molecules assembled together to form an agglomeration of various sizes (Fig. 1E), which confirmed the results of DLS. MPDA NPs exhibited a well-defined spherical morphology and mesoporous structure (Fig. 1F). In the M@S NPs, the mesoporous structure and surface of MPDA NPs was concealed by a layer of SS31 (Fig. 1G). This observation confirmed that the MPDA NPs can not only steadily attract SS31, but also divide SS31 particles from the agglomeration and significantly improve the disordered distribution. The SS31 loading capacity was quantified. According to the standard curve (Fig. S1), the loading content of SS31 by 1 mg MPDA NPs was approximately 0.096 mg. Furthermore, a molecular docking study was performed to investigate the binding mode of M@S NPs. PDA NPs were fabricated via dopamine oxidation, and are usually considered to include four types of monomers [50]. For convenience, we named these monomers DA1, DA2, DA3, and DA4 according to the oxidation degree from low to high. DA1 was dopamine, the unoxidized monomer, and DA4 was 5,6-indolequinone, the highest oxidized product among these monomers [51]. The four monomers docked into the binding site of SS31 and the results are shown in Fig. 1H. The compound monomers adopted compact conformations to bind at the site of SS31. Detailed analysis showed that different numbers of hydrogen bonds with different bond lengths were formed between the four monomers and SS31. The maximum binding affinity between DA1, DA2, DA3, or DA4 and SS31 were predicted to be −3.3, −3.1, −3.0 and −2.9 kcal/mol, suggesting that the stability order was SS31–DA1 > SS31–DA2 > SS31–DA3 > SS31–DA4. The above molecular simulations provide a rational explanation of the interactions between the four monomers and SS31, which indicated that M@S NPs could release SS31 in response to ROS with the oxidation of MPDA NPs. To further evaluate the stability, SS31 with the unoxidized monomer DA1 and the highest oxidized monomer DA4 were analyzed by 100-ns molecular dynamics simulations based on the docking results. The two monomers were first docked into the binding site of SS31 and then molecular dynamics refinements were performed; results are shown in Fig. 1I. The compound monomers adopted compact conformations to bind at the site of the peptide. Detailed analysis showed that different numbers of hydrogen bonds with different bond lengths were formed between the two monomers and SS31 (Fig. 1I). In addition, the total binding free energy of the SS31–DA4 complex and the SS31–DA1 complex was calculated according to the MMGBSA approach, and the estimated ΔGbind was found to be −3.98 kcal/mol for SS31–DA4 and -5.59 kcal/mol for SS31–DA1, suggesting that the SS31–DA1 complex was more stable than the SS31–DA4 complex. Furthermore, spectrofluorimetry was used to elucidate the ROS-responsive release of M@S NPs. The results showed that the amount of SS31 released from MPDA NPs increased with increasing ROS concentration (Fig. S2), which was consistent with the previous experimental data. In addition, MPDA NPs are pH-responsive delivery drugs and are widely used for cancer treatment [52]. However, due to exposure to internal body fluids or infection, the pH of a chronic wound will elevate to become slightly alkaline [53]. In diabetic wounds, this weakly alkaline environment will reduce chemical degradation of M@S NPs and prolong their function [54]. In summary, these results demonstrated that we succeeded in constructing M@S NPs and that the NPs responded to ROS.

3.2. Preparation and characterization of hydrogel

A multi-crosslinked double-network hydrogel was composed of F127DA and HAMA. HA is a crucial component of the ECM [55]. The addition of methacrylate to the HA backbone means that HAMA not only has significant biocompatibility and biodegradability, but also possesses the ability to photopolymerize when exposed to suitable wavelength ultraviolet (UV) light [56]. However, we found that the HAMA gel did not meet clinical wound dressing requirements. In diabetic wounds, with increased hyaluronidase activity and rising ROS levels, HA will be rapidly fragmented and degraded [6,57]. Furthermore, approximately half of diabetic ulcers are plantar ulcers, while most non-plantar ulcers occur in the toes, ankles and elbows [17,48]. In order to effectively deliver drugs, more attention should be paid to the mechanical properties of a hydrogel. For example, a hydrogel needs to be adhesive to give it the ability to consistently release drugs within the wound [58], while its compression and recovery properties must be adequate to prevent mechanical rupture [48]. To meet these requirements, we designed a composite hydrogel where F127DA micelles were introduced into the HAMA network (Fig. 2A). PF127 is an amphiphilic triblock polymer, which is widely used due to its superior mechanical characteristics [59]. First, the mechanical properties and biocompatibility of different concentrations of F127DA (F) or HAMA (H) were evaluated. As shown in Figs. S3A and S3B, the mechanical properties of double-network hydrogel were far ahead of single-network hydrogel, and increasing the concentration of F or H strengthened the mechanical properties but high concentrations of H decreased the toughness of the hydrogel. The biocompatibility of hydrogels is shown in Fig. S4. Compared with 5% F+1%H (5 wt% F127DA and 1 wt% HAMA) and 10%F+1%H, the 15% F+1%H group contained more dead cells and cell agglomerations, as did the 10%F+0.5%H group, compared with 10%F+1%H and 10%F+2%H. These results indicated that the mechanical properties of the double-network hydrogel were superior to those of the single-network hydrogel, and although increasing the concentration of F or H will enhance the mechanical properties, a high concentration of F will reduce biocompatibility while a high concentration of H will decrease the toughness. In summary, a concentration of 10% F and 1% H produced a good balance between the mechanical properties and biocompatibility, which was also in agreement with a previous study which showed that concentrations of 10% F and 1% H resulted in superior photo-initiated velocity, flexibility, and drug release rate [60]. Consequently, this concentration was chosen for subsequent experiments. A gross view of the UV-crosslinking procedure of the four gels (FH hydrogel, FH–SS31 hydrogel, FH–MPDA hydrogel, and FH–M@S hydrogel) is shown in Fig. 2B.

To examine the mechanical properties of these hydrogels, the compression and recovery properties were tested. First, each hydrogel was fabricated into columns, then compression tests were carried out over the range of 0–60% of strain. The test results of the initial state, 30% strain, 60% strain and recovered state were recorded (Fig. 2C). Compression stress–strain curves are shown in Fig. 2D. These hydrogels withstood compression without breaking, and after the compression was released, the hydrogels recovered rapidly to their initial shape. We calculated the elastic modulus of the hydrogels from the stress–strain

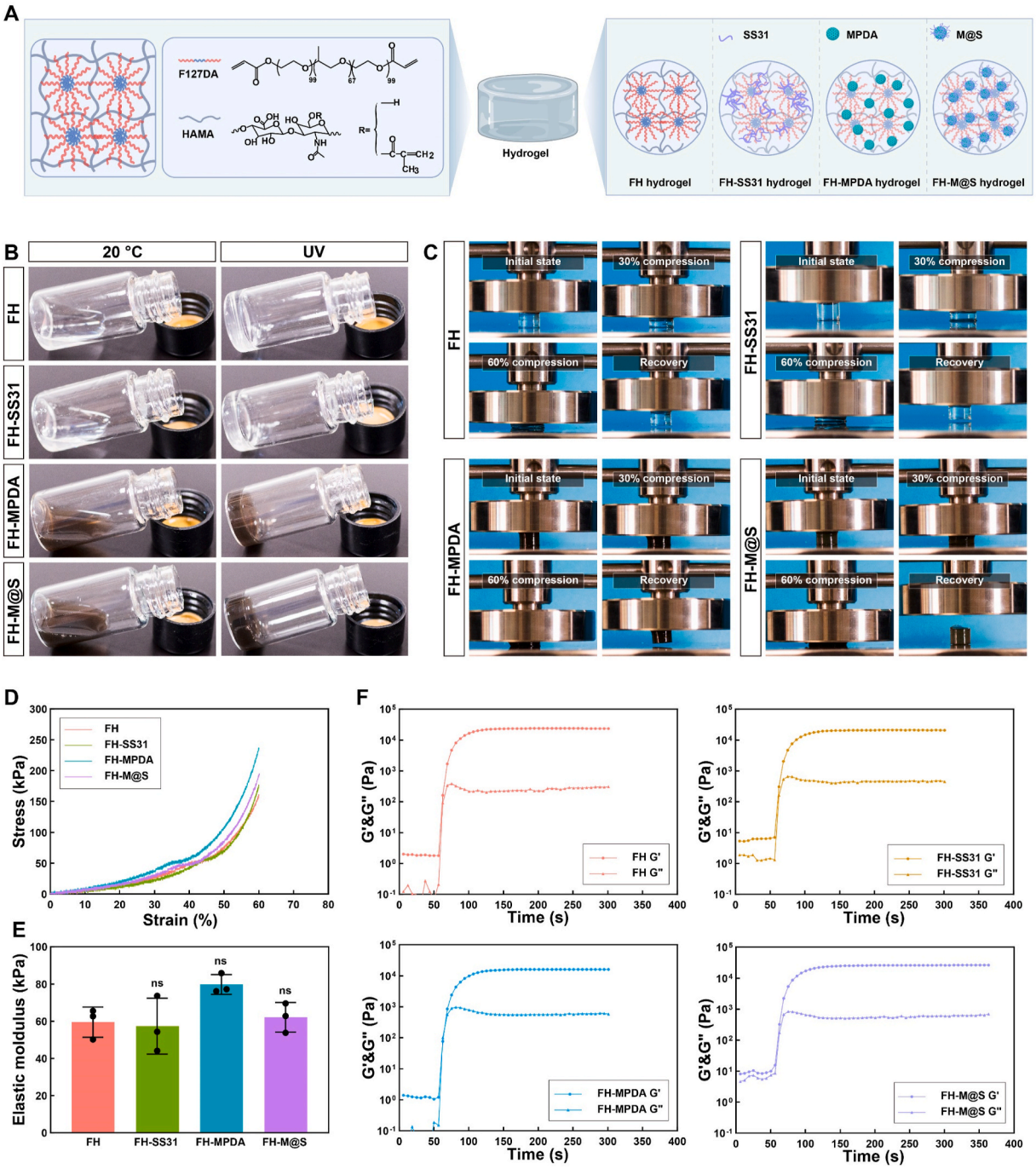

Fig. 2. Characteristics of FH, FH–SS31, FH–MPDA, and FH–M@S hydrogels. (A) Schematic illustration of the elements of the four types of hydrogels. This illustration was created with BioRender.com. (B) Photographs of the hydrogel precursor solutions and the corresponding hydrogels. (C) Photographs of the compression process: initial state, 30% compression, 60% compression, and recovery. (D) Compressive stress–strain curve of the four types of hydrogels. (E) Elastic modulus of the four types of hydrogels. Data are expressed as mean ± SD (n = 3). (F) Rheological performance of the hydrogels, after exposure to 405 nm ultraviolet light.

curves and the elastic moduli of FH hydrogel, FH–SS31 hydrogel, FH–MPDA hydrogel, and FH–M@S hydrogel were 59.47 ± 6.66 kPa, 57.36 ± 12.25 kPa, 79.72 ± 4.34 kPa and 62.05 ± 6.49 kPa respectively, as shown in Fig. 2E. To further determine whether the content in the gel affects its gelling abilities, a dynamic rheological test of the gels was used to quantitatively describe its sol–gel transition. The oscillatory time sweep curve was measured, and when the hydrogels were exposed to 405 nm UV light at 56 s, all four hydrogels were immediately transformed into the gel state over approximately 60 s. As shown in the results (Fig. 2F), the storage moduli (G′) of the FH, FH–SS31, FH–MPDA and FH–M@S were 23.7 kPa, 20.9 kPa, 16.1 kPa and 26.2 kPa respectively. These data indicated that due to the negative charges of the MPDA and the positive charges of the SS31, the rheological properties of the hydrogels might be impacted by the potentials, while the rheological property of the hydrogel containing M@S NPs remained steady because the potential of the M@S NPs was close to neutral. Interestingly, for the precursors of all four types of hydrogels (before exposure to UV), G′ was slightly greater than the loss moduli (G"). Previous studies indicated that F127, a temperature-sensitive hydrogel, exhibited this phenomenon (G' > G"), at a suitable concentration and temperature [61,62]. F127DA, with two vinyl groups added onto the ends of the F127 chain, retains the PEO-PPO-PEO tri-block copolymer structure of F127 [49,63], so

F127DA might also show the same rheological feature as F127.

Diabetic wounds usually occur in a variety of shapes, and thus, compared with pre-formed gels, *in situ* cross-linkable gels should be better able to fully seal the wounds when injected into the wound, protecting the wound from infection, while also delivering drugs [64]. As shown in Figs. S5A and S5B, within a few seconds after transitory photo-crosslinking, the hydrogels and the hydrogel precursor solutions could be extruded from a syringe, and thus they could be used to cover any shape of irregular diabetic skin defect. The gels adhered onto the wound without any extra assistance such as bandages or 3 M adhesives [65]. Furthermore, the gels with superior adhesive properties were easy to apply and use in physical excision [48,66]. The adhesion of the four gels were assessed. These gels were used to adhere two pieces of rat skin and the results showed that the skins were closely and firmly adhered by the gels and withstood 100 g loads (Fig. S6A). Furthermore, the lap-shear test was used to estimate the adhesion of the four gels. As shown in Fig. S6B, all groups showed similar maximum adhesive forces, with the exception of the FH–MPDA group. These data indicated that hydrogel adhesion might also be impacted by the surface potential. As mentioned in regard to dynamic rheological testing of hydrogels, the negative charges of the MPDA NPs and the positive charges of the SS31 also impacted hydrogel adhesion, while the potential of the M@S NPs was close to neutral and minimized the impact. All the data indicated the excellent mechanical properties of the FH hydrogel and also demonstrated that the mechanical properties would not be impacted by the M@S NPs. Hence, based on these properties, the gels containing M@S NPs were found to meet most of the mechanical property requirements for wound dressing.

3.3. Photothermal performance of M@S NPs in hydrogel

To examine the photothermal performance of M@S NPs, the changes in temperature of hydrogels containing M@S NPs were recorded by infrared imaging, after exposure to a laser (808 nm) for 5 min (Fig. 3A). With increasing power densities of 0.1 W/cm^2, 0.3 W/cm^2, 0.5 W/cm^2 and 0.7 W/cm^2, the temperature of the hydrogel increased to 28.8 °C, 35.1 °C, 38.5 °C and 47.2 °C respectively (Fig. 3B). Next, the temperature of the hydrogel rapidly increased and then decreased, after exposing it to NIR and then turning off the laser (Fig. 3C). The results of this test suggested that M@S NPs had good photothermal conversion efficiency and good safety so that the skin of a patient will not be burned owing to continued heating after turning off the laser. Next, the photothermal stability of M@S NPs was tested. The hydrogel was exposed to four cycles of heating and cooling and the photothermal performance of M@S NPs was near identical (Fig. 3D), confirming the photothermal stability of M@S NPs and the heat resistance of the hydrogel [67]. In addition, the FH, FH–SS31, FH–MPDA, and FH–M@S hydrogels were treated with NIR. The temperature change curves are shown in Fig. 3E and the infrared thermal images of FH hydrogel and FH–M@S hydrogel, for example, are shown in Fig. 3F. The results showed that MPDA and M@S NPs exhibited similar photothermal capacity and indicated that the photothermal capacity of MPDA NPs was not impacted by the

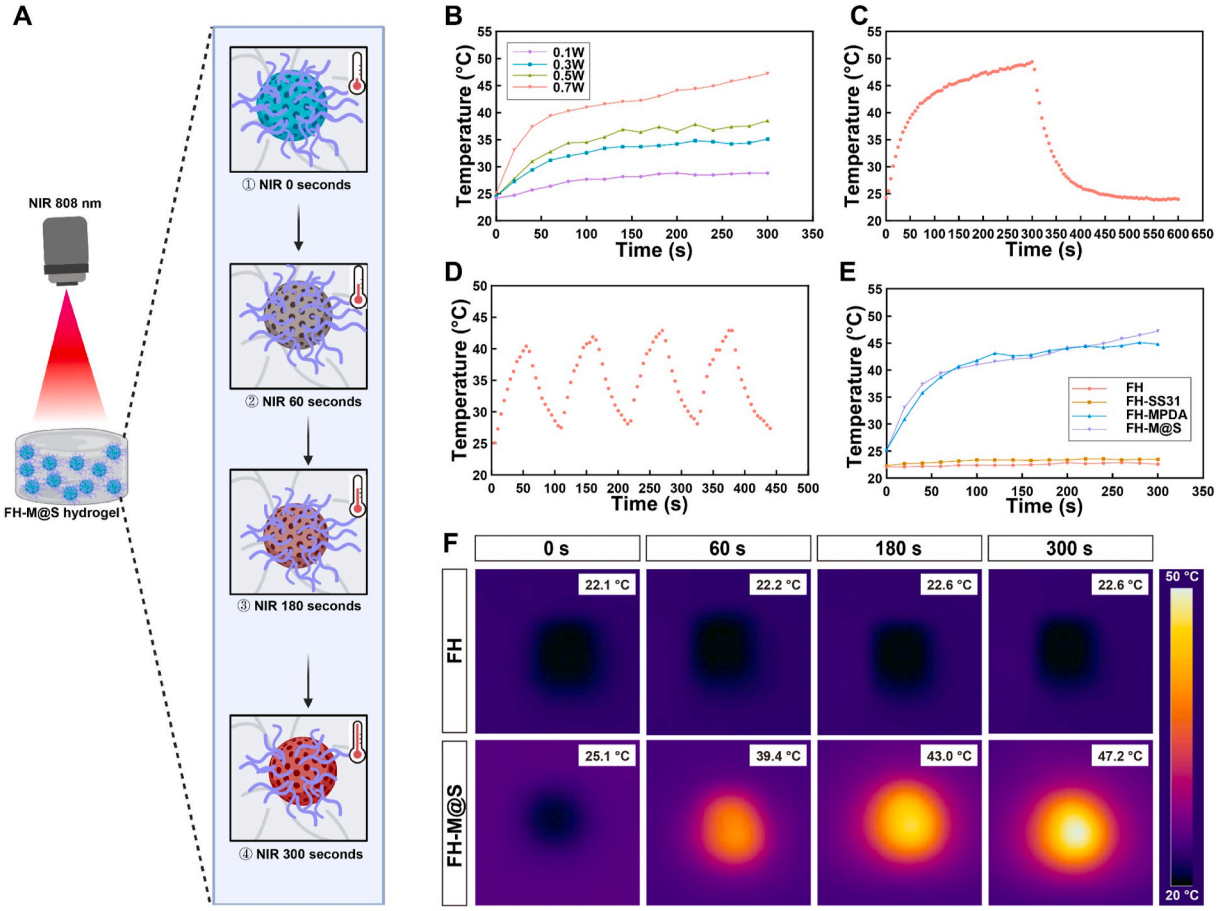

Fig. 3. Photothermal effect of the four types of hydrogels. (A) Diagram of the photothermal process. This illustration was created with BioRender.com. (B) Laser intensity–dependent temperature change curves of FH-M@S hydrogel with NIR (0.1, 0.3, 0.5, and 0.7 W/cm^2). (C) "On−off" temperature change of FH–M@S hydrogel under 0.7 W/cm^2 laser irradiation for 5 min. (D) Photothermal stability of FH–M@S hydrogel over four consecutive photothermal heating (0.7 W/cm^2) and natural cooling cycles. (E) Temperature change curves of the four types of hydrogels. (F) Infrared thermal images and central temperature of FH and FH–M@S hydrogels irradiated by 0.7 W/cm^2 laser at 0 s, 60 s, 180 s, and 300 s.

attachment of SS31. These data demonstrated that the M@S NPs possessed superior photothermal capacity and were competent to act as anti-bacterial agents.

3.4. Antibacterial properties of FH–M@S hydrogel in vitro

In the treatment of diabetic wounds, bacterial infection is one of the most common and thorny challenges, which causes increases in ROS level, up-regulation of the expression of proinflammatory cytokines, and degradation of ECM and growth factors [68–71]. Based on the above impactful photothermal properties of M@S NPs, the NPs were recognized as rapid, efficient, and broad-spectrum antibacterial agents [19]. In this study, the antibacterial performance of M@S NPs was evaluated *in vitro*. The classical gram-positive bacterium *Staphylococcus aureus* (*S. aureus*), and gram-negative bacteria *Escherichia coli* (*E. coli*) and *Pseudomonas aeruginosa* (*P. aeruginosa*) were cultured with M@S NPs and spread on plates, after treatment with or without NIR (808 nm), to characterize the antibacterial properties, as shown in Fig. 4A. In the NIR experiments, the laser power was 0.7 W/cm^2 and irradiation was performed for 10 min. As shown in Fig. 4B, in the absence of laser irradiation, the blood plates were occupied by a large number of colony-forming units, demonstrating that the antibacterial properties against *S. aureus*, *E. coli*, and *P. aeruginosa* were very weak. In contrast, after laser irradiation, the MPDA group and M@S group both exhibited significant antibacterial activity and the number of colonies of all three bacteria were remarkably decreased. Furthermore, the antibacterial properties of hydrogels were evaluated by bacterial Live/Dead staining assay. As shown in Fig. S7, in the FH group and the FH–SS31 group only a few red fluorescent dots were visible, while in the FH–MPDA group and the FH–M@S group many dense red fluorescent dots were evident, indicating that there were a large number of dead bacteria in the FH–MPDA group and the FH–M@S group after exposure to NIR. These results indicated that when the MPDA NPs were exposed to NIR, as a result of the high NIR absorbance and excellent photothermal

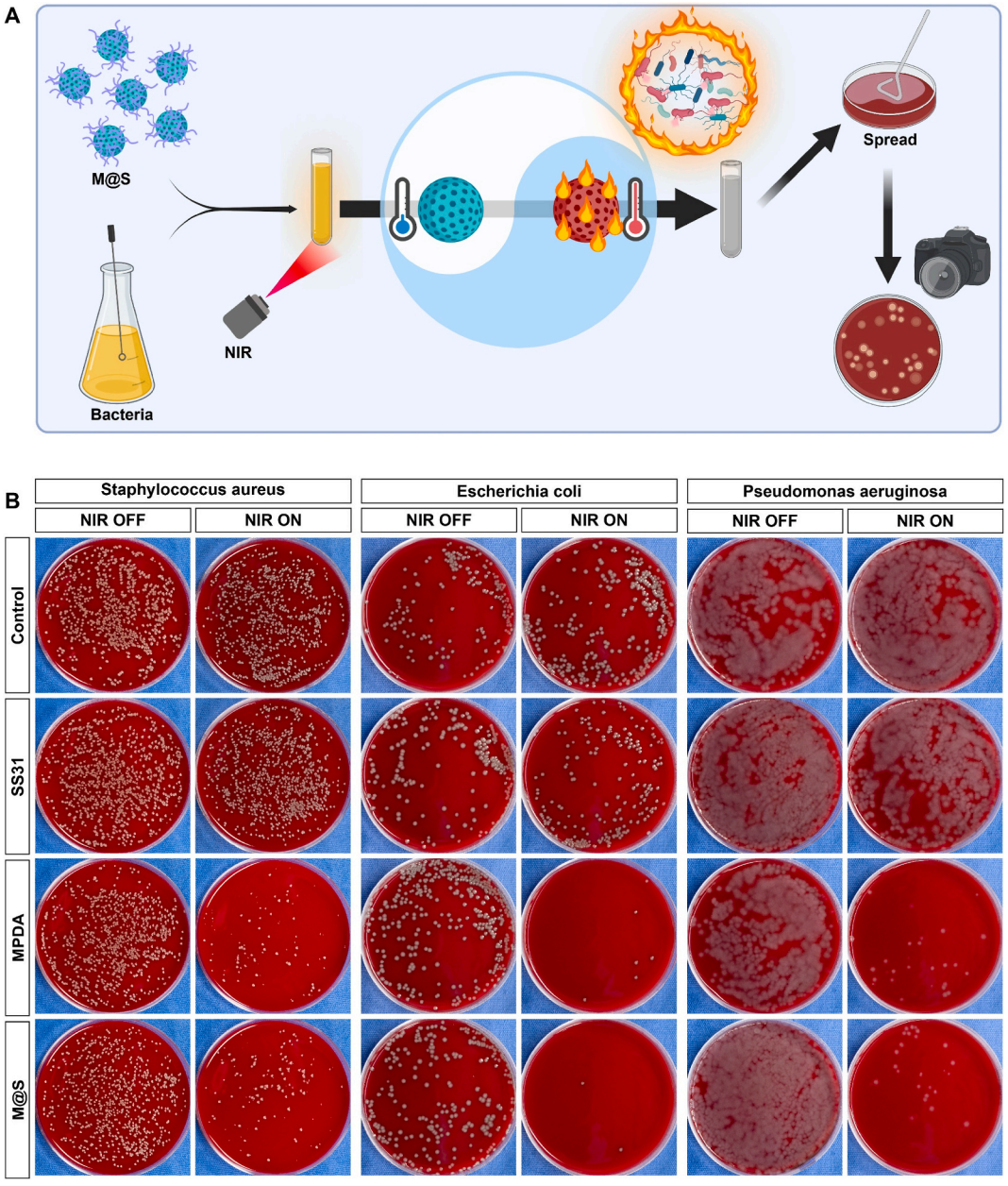

Fig. 4. *In vitro* antibacterial properties of M@S NPs under NIR irradiation (808 nm, 0.7 W/cm^2). (A) Schematic diagram showing the photothermal antibacterial process. This illustration was created with BioRender.com. (B) Photographs of bacterial colony plate counting after exposure to NIR for 10 min.

conversion of the MPDA NPs [72], the temperature of the bacterial culture rapidly increased and the majority of microorganisms suffered irreversible damage caused by a great deal of protein denaturation and release of various enzymes [40,41]. Moreover, similar to tannic acid, the MPDA NPs were resistant to bacterial infection by contact-active mechanisms in that many membrane metallic ions, playing a role in bacterial metabolism and some heteromeric proteins, would be chelated by the catechol, causing disruption of the bacterial structure to achieve the antibacterial effect [41,73].

After exposure to NIR, the temperature of the hydrogel increased to approximately 45 °C, a mild temperature, which not only effectively kills bacteria and reduces necrosis of normal cells [74,75], but also promotes blood circulation and angiogenesis in wounds [76,77]. In addition, shining a low-level laser onto the wound will enhance the proliferation, differentiation, and migration of fibroblasts and endothelial cells, and increase collagen deposition and neovascularization [78,79]. Collectively, exposure to NIR, mild heat and low-level laser therapy can combat bacteria and accelerate wound healing.

3.5. Release, cell uptake, and mitochondrial targeting of SS31 in vitro

As mentioned earlier, SS31 is a mitochondria-targeting peptide which attaches to the mitochondrial inner membrane, resulting in the acyl chains of cardiolipin not contacting cytochrome C [72]. Consequently, the rate-limiting step of the ETC, with cytochrome C acting as an electron carrier commuting between complex III and complex IV, can proceed smoothly, especially under hyperglycemic conditions [13,22]. In addition, the efficiency of electron transport, OXPHOS, and the production of ATP, all improve, electron leaks are reduced and the output of ROS is decreased (Fig. 5A) [13,80].

In order to investigate cell uptake and the mitochondrial targeting ability of SS31, we prepared FITC-labeled SS31 (SS31-FITC). After

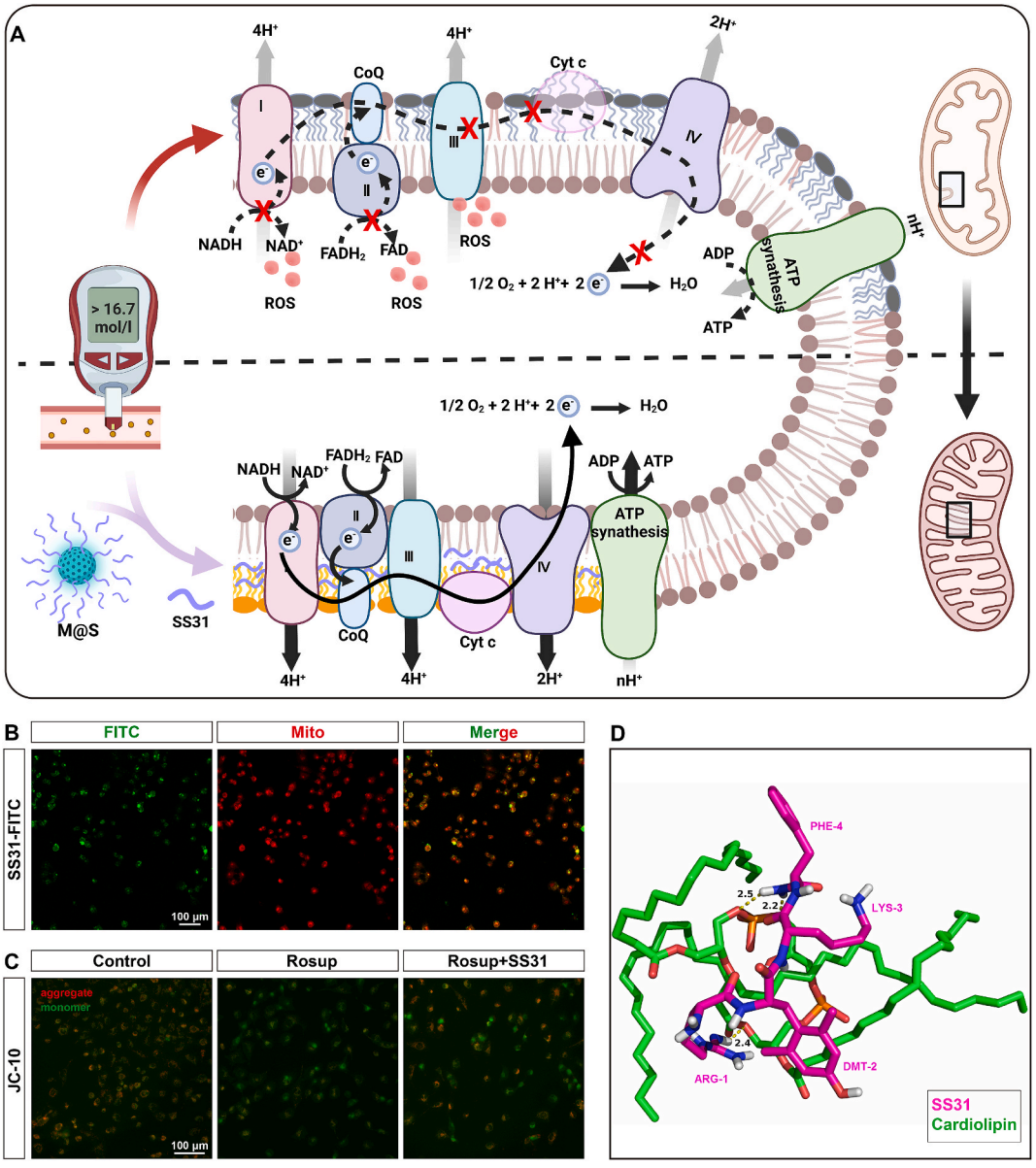

Fig. 5. Targeted uptake and mechanisms of action of SS31. (A) Schematic diagram showing the mechanism of SS31. This illustration was created with BioRender.com. (B) Representative confocal images of cellular uptake of SS31-FITC. SS31-FITC is shown in green, and mitochondria are shown in red. Scale bar, 100 μm. (C) Fluorescence microscopic images of JC-10 assay to measure mitochondrial membrane potential in Rosup-stimulated cells after different treatments. The red fluorescence represents JC-10 aggregates and the green fluorescence represents JC-10 monomers. Scale bar, 100 μm. (D) SS31 (purple sticks) docked into the binding site of cardiolipin (green sticks).

treatment of cells with SS31-FITC, confocal laser scanning microscopy (CLSM) was used to observe the outcome. As shown in Fig. 5B, the green fluorescence (SS31) and red fluorescence (Mito-Tracker) could be merged together. These results indicated that SS31 could be taken up by cells and targeted to mitochondria. Next, the JC-10 assay was used to evaluate the effect of SS31 on mitochondrial membrane potential. As shown in Fig. 5C, when Rosup, a ROS-inducing agent [81,82], was added into the cell culture medium to imitate high-glucose conditions with high levels of ROS, much of the JC-10 monomer (green) could not agglomerate into JC-10 aggregates (red) in the mitochondrial matrix, while when SS31 was added into the Rosup-supplemented cell culture medium, SS31 inhibited the effects of Rosup and enhanced the mitochondrial membrane potential [83,84]. Furthermore, we used molecular docking analysis to confirm the binding between cardiolipin and SS31.

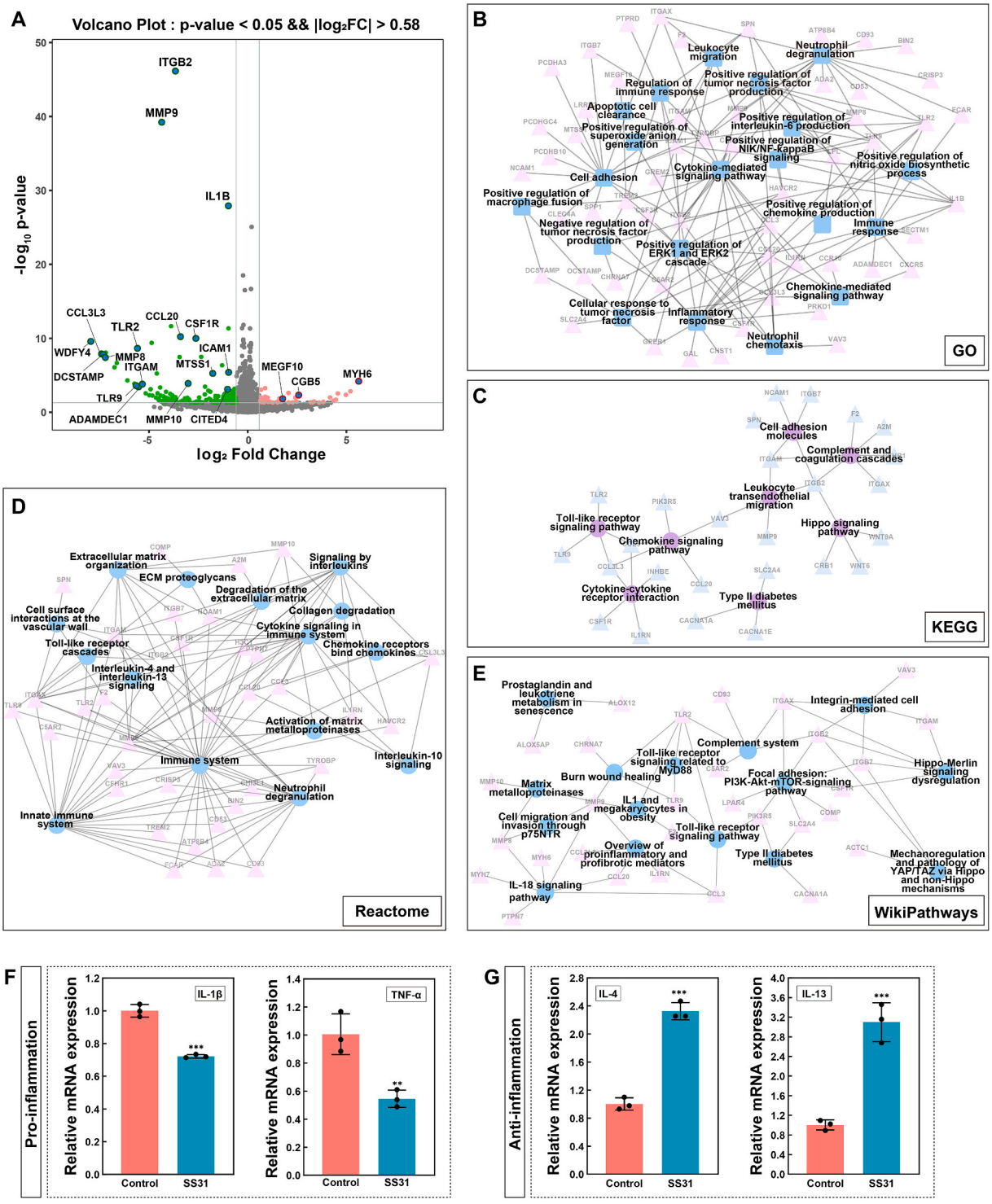

Fig. 6. Exploring the biological functions of SS31. (A) Volcano plot visualization of the differentially-expressed genes in response to SS31 treatment. (B, C, D, E) The results of GO, KEGG, Reactome, and WikiPathways pathway enrichment analysis after RNA sequencing (RNA-seq). (F, G) The relative mRNA expression level of pro-inflammatory cytokines (IL-1β and TNF-α) and anti-inflammatory cytokines (IL-4 and IL-13) after treatment with SS31. Data are expressed as mean ± SD (n = 3). **, $p < 0.01$ compared with the control group, and ***, $p < 0.001$ compared with the control group.

As shown in Fig. 5D, the estimated binding energy was −4.5 kcal/mol. SS31 adopted a compact conformation to bind at the site of the cardiolipin. The fatty chain of the cardiolipin formed strong hydrophobic interactions with the residue Phe-4 of SS31. Detailed analysis showed that three hydrogen bond interactions formed between the cardiolipin and the SS31 (bond lengths: 2.4, 2.2, 2.5 Å), which was the main interaction between the cardiolipin and the SS31. Above all, these data showed that the SS31 attached to MPDA NPs entered into mitochondria and interacted with cardiolipin in the mitochondrial inner membrane thus enhancing mitochondrial function.

3.6. Exploring the biological functions of SS31

To further determine the potential molecular mechanisms of SS31, RNA sequencing (RNA-seq) was used to explore the changes in HMEC-1 after treatment with SS31. As shown in the volcano plots (Fig. 6A), we identified 156 significant differentially-expressed genes (DEGs), of which 31 were upregulated and 125 were downregulated. These DEGs were then used for pathway enrichment analysis. The GO (Fig. 6B), KEGG (Fig. 6C), Reactome (Fig. 6D), and WikiPathways (Fig. 6E) analysis all revealed the involvement of several inflammatory signaling pathways, including Toll-like receptor signaling (TLR) pathway and NIK/NF-kappaB signaling, many inflammation factor signaling pathways, such as tumor necrosis factor (TNF), interleukin (IL)-1, IL-18, IL-4, IL-10, and IL-13, and matrix metalloproteinases (MMPs). Moreover, there were also many ECM-related pathways, such as ECM organization, cell surface interactions at the vascular wall, collagen degradation, ECM proteoglycans, and ECM degradation. In addition, these databases tipped some cell proliferation and apoptosis signaling pathways, such as positive regulation of ERK1 and ERK2 cascades, PI3K-Akt-mTOR-signaling pathway, and apoptotic cell clearance. Moreover, we found some interesting signaling pathways: type II diabetes mellitus and burn wound healing. This pathway enrichment analysis of the DEGs indicated that SS31 regulates the inflammatory response and impacts cell proliferation and apoptosis. Next, qRT-PCR assays were used to confirm the changes in the expression levels of inflammation-related cytokines. As shown in Fig. 6F and G, SS31 significantly decreased expression of the pro-inflammatory cytokines, IL-1β and TNF-α, and strikingly enhanced expression of the anti-inflammatory cytokines, IL-4 and IL-13. Meanwhile, western blotting showed that after treatment with SS31, the quantity of IκB-α, an NF-κB inhibitor, was increased (Fig. S8). A previous study reported that inhibiting the MyD88-dependent TLR pathway inhibits activation of IRAK family kinases, self-ubiquitination of TRAF-6 and activation of ubiquitin-dependent kinase, subsequently inhibiting the activation of IκB kinase (IKK) which results in the phosphorylation and degradation of IκB-α [85]. With the decreased degradation of IκB-α, IκB-α inhibits the activation of NF-κB, leading to decreased expression of pro-inflammatory cytokines. Combining the results of RNA-seq, qRT-PCR, and western blotting, we speculated that SS31 might inhibit the MyD88-dependent TLR pathway, inhibit the degradation of IκB-α, and decrease the expression level of pro-inflammatory cytokines. In addition, SS31 was found to associate strongly with the signaling pathway of PI3K-Akt-mTOR, which plays crucial roles in regulating vascularization [86,87], and promotes M2 macrophage polarization to secrete anti-inflammatory factors [88]. As shown in Fig. 6G and Fig. S8, SS31 upregulated the phosphorylation levels of Akt and mTOR and enhanced the expression level of IL-4 and IL-13. These results indicated that SS31 activated angiogenesis-associated signaling pathways, upregulated expression of pro-angiogenic factors, and promoted angiogenesis. Consequently, we concluded that SS31 could be used to manage diabetic wound healing by inhibiting inflammation and apoptosis and promoting cell proliferation and angiogenesis.

3.7. Migration, antioxidation, vascularization, and macrophage polarization of M@S NPs

Cell migration plays a crucial role in wound healing, for example, endotheliocyte migration promotes vascularization and fibrocyte migration accelerates wound closure [89]. To ascertain the impacts of M@S NPs on cell migration, the transwell assay was used to assess the effect of M@S NPs on migration of HMEC-1 and HFF-1. After HMEC-1 and HFF-1 passed through the transwell membrane and adhered to the lower surface, the membranes were stained with crystal violet and the results and experimental procedure are shown in Fig. 7A and B. Compared to the control group, both HMEC-1 and HFF-1 treated with SS31, MPDA NPs, or M@S NPs showed enhanced migration, with the M@S group showing the best effect followed by the MPDA group and the SS31 group (Fig. S9). These effects may be caused by SS31 increasing the production of ATP which enhances migration of fibroblasts and endothelial cells [90,91], while the bioactive functional groups of MPDA NPs, such as quinone and phenolic hydroxyl groups, promote cell adhesion and migration [92,93]. The M@S NPs have superior ability to protect cells from damage by ROS, because of their properties of scavenging ROS and reducing production of mtROS [23,24,94]. To confirm the ROS-scavenging property of M@S NPs *in vitro*, 2′,7′-dichlorofluorescein diacetate (DCFH-DA), a fluorescent probe of ROS, was used to evaluate the intracellular ROS level, after HMEC-1 were stimulated by Rosup. The results showed that levels of ROS were low under normal conditions, while the level of ROS was dramatically increased following stimulation with Rosup. After treatment with SS31, MPDA NPs, or M@S NPs, the levels of ROS significantly decreased (Fig. 7C), indicating their excellent antioxidative activity. Under chronic hyperglycemic conditions, a large number of ROS were produced and in order to mimic a pathologic setting, the effects of M@S NPs in inhibiting cell death were investigated under high-ROS conditions. Therefore, Rosup was added to cell culture medium to induce cell death by promoting ROS production, and the Live/Dead assay was used to evaluate the ability of M@S NPs to inhibit cell death. After treatment with Rosup, cell death would be induced in the Rosup group, and morphological analysis of residual cells showed they were curled up into a ball. In contrast, in the Rosup + SS31, Rosup + MPDA, and Rosup + M@S groups, only a few cells appeared apoptotic (Fig. 7C). These results indicated that SS31, MPDA NPs, and M@S NPs all inhibited cell death efficiently. Next, the effects of M@S NPs on vascularization *in vitro* by HMEC-1 were also investigated after Rosup treatment. As shown in Fig. 7C and Fig. S10, all cells were cultured on Matrigel, and all treated with Rosup except the control group. The results showed that HMEC-1 cells of the control group migrated and self-assembled into capillary-like networks. Under ROS-inducing conditions, the tube formation ability of HMEC-1 was significantly reduced. In contrast, when cells were cultured on Matrigel with M@S NPs, the effects of Rosup were reversed and the mesh formation abilities of HMEC-1 were restored. In diabetic wounds, persistent inflammation is in large part caused by dysregulated macrophage polarization [89]. Consequently, the effects of M@S NPs on macrophage polarization were also investigated. As shown in Fig. 7D and Fig. S11, compared with the control group, SS31, MPDA NPs, and M@S NPs significantly downregulated the expression of iNOS (a marker of M1-like macrophages) and induced the expression of CD206 (a marker of M2-like macrophages), with the effects being most marked in the M@S NPs group. These findings indicated that M@S NPs strikingly enhanced M2 macrophage polarization and suppressed M1 macrophage polarization.

3.8. Biocompatibility, antioxidation and macrophage polarization of FH–M@S hydrogel in vitro

Next, we evaluated the biocompatibility of these hydrogels *in vitro*. After co-culture for 3 days, the Live/Dead assay showed that there were no obvious differences between any of the groups, most cells exhibited green fluorescence and few dead cells were present (Fig. 8A). Scanning

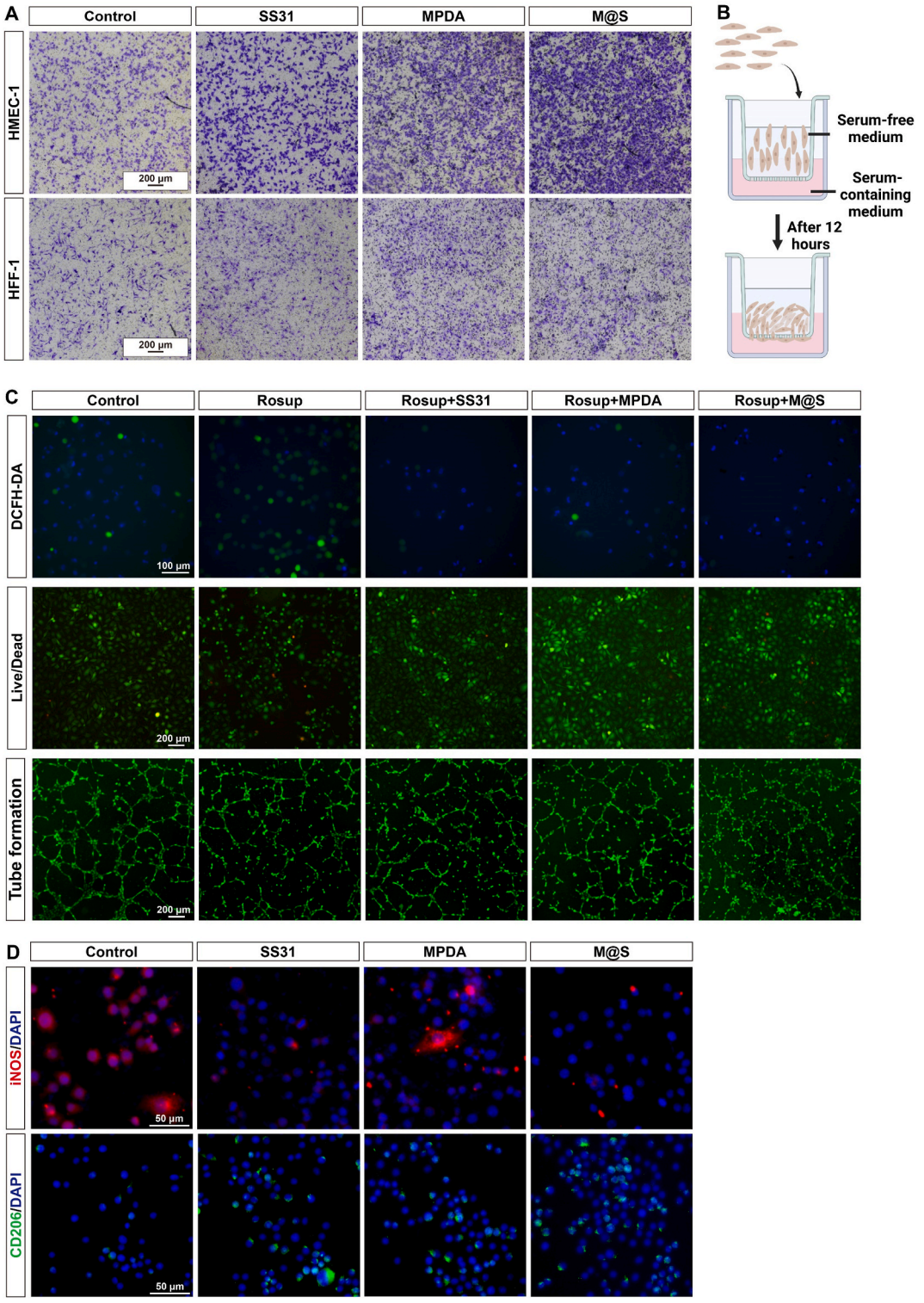

Fig. 7. Biological effects of M@S NPs *in vitro*. (A) Evaluation of migration of HMEC-1 and HFF-1 treated with different substrates for 12 h. Scale bar, 200 μm. (B) Schematic diagram showing performance of the transwell assay. This illustration was created with BioRender.com. (C) Fluorescence images of intracellular ROS analysis with DCFH-DA in Rosup-stimulated cells after different treatments. Scale bar, 100 μm. Fluorescence images of the Live/Dead assay revealed the anti-apoptosis effect of Rosup stimulation in cells after different treatments. Scale bar, 200 μm. Tube-formation assay of HMEC-1 in Rosup-stimulated cells after different treatments. Scale bar, 200 μm. (D) Fluorescence images of macrophage polarization after different treatments (red: iNOS; green: CD206; blue: cell nuclei). Scale bar, 50 μm.

electron microscopy (SEM) was used to check the adhesive ability of cells seeded onto different hydrogels. As shown in Fig. S12, HMEC-1 attached onto the surface of all hydrogels, and in the FH–M@S hydrogel group, there were many intercellular links between adjacent cells. These data illustrated that the FH–M@S hydrogel has excellent cytocompatibility and provides a good environment for cell growth. Furthermore, the co-culture methods for hydrogel and cells were used to assess the ROS-scavenging property of FH–M@S hydrogel (Fig. 8B and

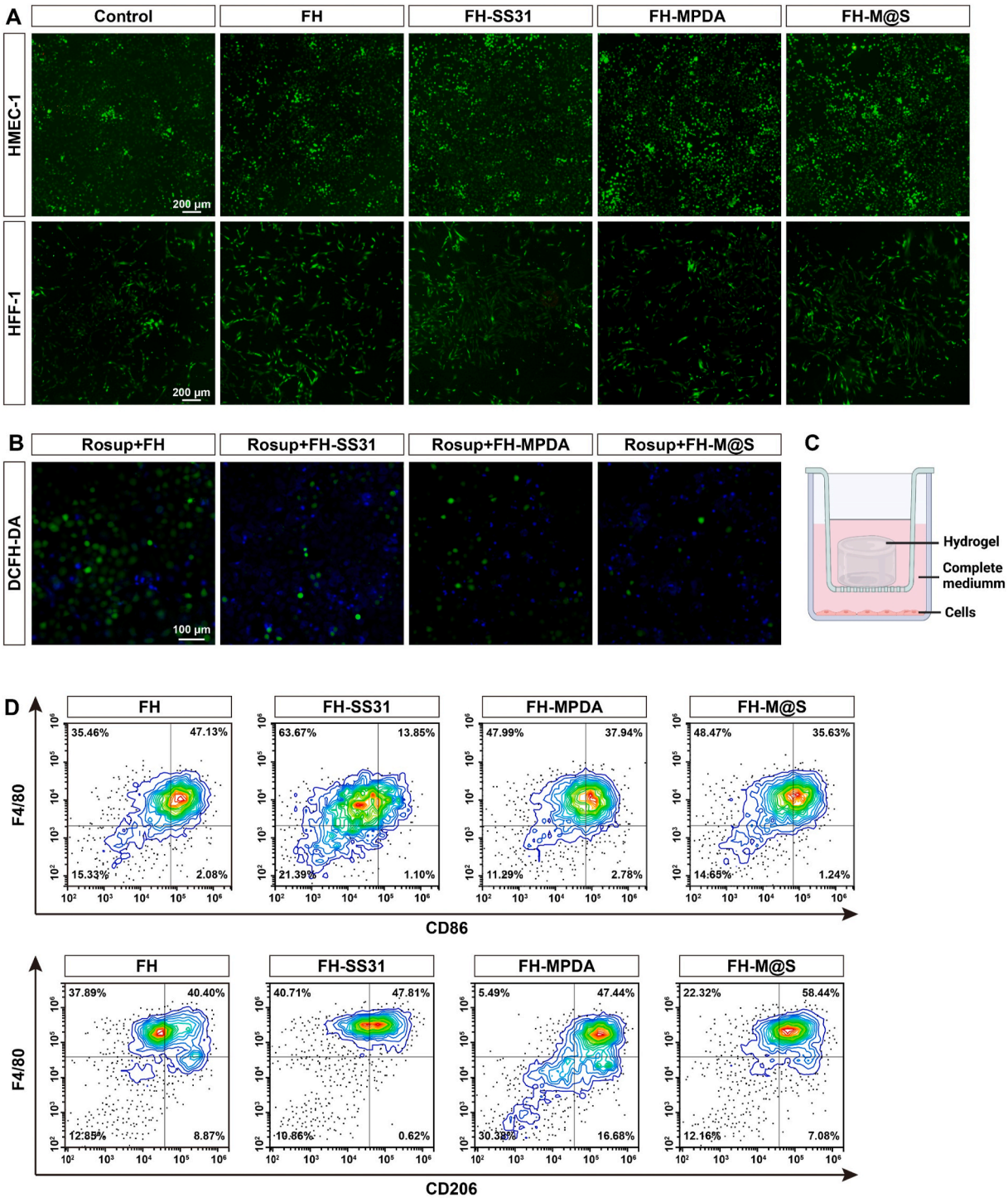

Fig. 8. Biocompatibility and biological effects of FH–M@S hydrogel *in vitro*. (A) Live/Dead staining of HMEC-1 and HFF-1 with different hydrogels after co-culture for 3 days. Scale bar, 200 μm. (B) Fluorescence images of intracellular ROS analysis with DCFH-DA in Rosup-stimulated cells after co-culture with different hydrogels. Scale bar, 100 μm. (C) Schematic diagram showing performance of the co-culture hydrogel and cells. This illustration was created with BioRender.com. (D) Flow cytometric analysis of M1 macrophage ($F4/80^+$ and $CD86^+$) and M2 macrophage ($F4/80^+$ and $CD206^+$) polarization after co-culture with different hydrogels.

C). The results showed that compared with FH hydrogel, the hydrogels containing SS31, MPDA NPs, or M@S NPs displayed antioxidative properties and the FH–M@S hydrogel was the best. In addition, the effect of FH–M@S hydrogel on macrophage polarization was assessed by flow cytometry (Fig. 8D). In M1 macrophage polarization, the FH–SS31 group displayed the lowest proportion of CD86-positive macrophages followed by the FH–M@S group and the FH–MPDA group, indicating the great effect of SS31 in inhibiting M1 polarization. Compared to the FH–M@S group, the FH–SS31 group showed significant superiority, which may be because SS31 was quickly released from the hydrogel to act on macrophages, while M@S NPs slowed the release of SS31 resulting in only some of the SS31 functioning. In M2 macrophage polarization, the FH–M@S group exhibited the best performance in promoting M2 macrophage polarization. These results showed that FH–M@S hydrogel has superior properties of inhibiting M1 macrophage polarization and promoting M2 macrophage polarization.

3.9. Diabetic wound healing performance of FH–M@S hydrogel in vivo

The incidence of diabetic wounds has been increasing and their prevention and treatment are considered one of the great challenges facing all countries in the world [95]. One of the main causes is the high oxidative stress level in the wound caused by diabetic hyperglycemia and bacterial infection [70,96]. Based on the aforementioned results, hydrogels containing M@S NPs with strong ROS scavenging capacity and antibacterial properties were used to treat diabetic wounds, to ascertain whether they could meet the requirements for augmenting diabetic wound healing. First, a diabetic SD rat model was established by intraperitoneal injection of streptozotocin (STZ) [97,98]. After successful establishment of the model, confirmed by blood glucose levels >16.7 mmol/L on two consecutive days after injection of STZ [99], a full-thickness wound model was established in diabetic rats. The wounds on each rat were distributed into five groups and were sealed with different wound dressings by application of different hydrogels using syringes, except for the control group which was covered with gauze with no other treatment. Then, these hydrogels were exposed to laser irradiation (808 nm, 0.7 W/cm^2) for 10 min, in order to simulate, in clinical application, the exposure of hydrogels to NIR, conferring on them the ability to kill bacteria and inhibit biofilm formation. The wound healing process was then observed and recorded on days 0, 5, 7, and 14 as shown in Fig. 9A and B, and the experimental procedure is shown in Fig. 9C. On day 5, the control group (87.84 ± 3.90% remaining) showed minimal healing and the FH group (77.24 ± 3.22% remaining) also showed only a weak effect on accelerating wound healing, while the groups treated with FH–SS31 hydrogel (62.59 ± 2.04% remaining) or FH–MPDA hydrogel (65.55 ± 4.15% remaining) both exhibited faster wound closure, and the size of the wound in the FH–M@S group, in which only 46.31 ± 1.55% of the wound area remained to be healed, was remarkably decreased compared with the

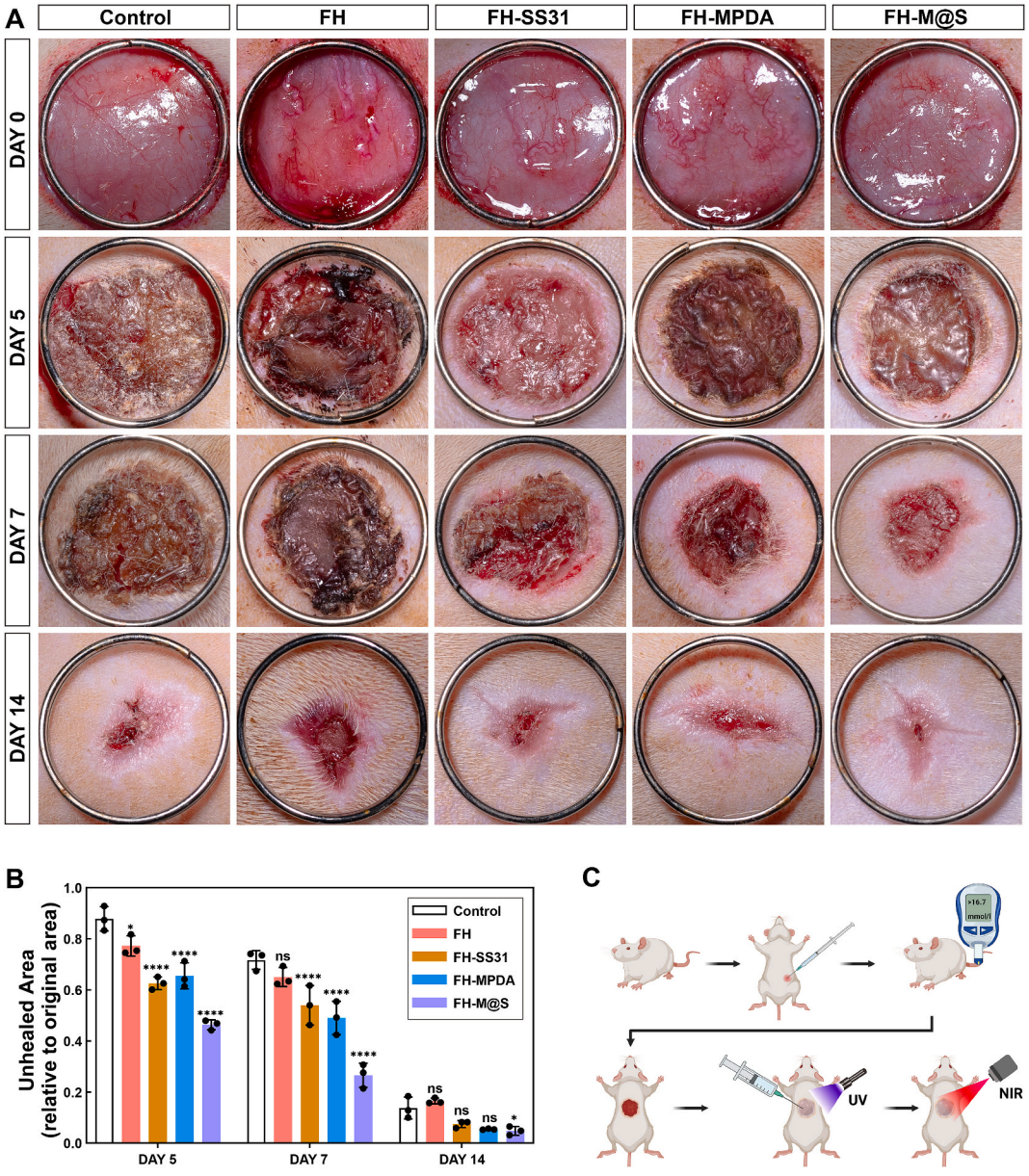

Fig. 9. FH–M@S hydrogel accelerated wound healing *in vivo*. (A) Representative photographs of diabetic cutaneous wounds of control, FH, FH–SS31, FH–MPDA, and FH–M@S hydrogel groups at days 0, 5, 7, and 14 after surgery. (B) Quantitative analysis of the unhealed area relative to the original area at day 5, day 7, and day 14 after surgery. Data are expressed as mean ± SD (n = 3). *, $p < 0.05$ compared with the control group, ****, $p < 0.0001$ compared with the control group. (C) Schematic diagram showing the experimental procedure *in vivo*. This illustration was created with BioRender.com.

other groups. On day 7, the wound healing-promoting properties of FH–M@S hydrogel, FH–SS31 hydrogel, and FH–MPDA hydrogel appeared more pronounced, especially the FH–M@S group which always exhibited the best wound closure effects, with only 26.57 ± 3.84% of the wound area remaining. After 14 days, although the wounds were almost closed in all groups, the wounds of the FH–M@S group were closest to fully healed. In the treatment of diabetic wounds, hydrogel seemed to be one of the most desirable candidates for wound dressing due to its similar structure to ECM, and properties including formation of a physical barrier and delivery of bioactive molecules [100,101]. Although there are many kinds of hydrogel available which exhibit various functions, many hydrogels failed to promote diabetic wound healing when applied *in vivo*, because a single-function hydrogel will not solve the multiple interconnected problems of nonhealing wounds [102]. To promote diabetic wound healing, many multi-functional hydrogels have emerged. For example, a bioactive hydrogel can deliver bioactive agents such as antibiotics, growth factors, and drug molecules, and an adhesive hydrogel can maintain close contact with a wound to prolong the acting time even in a wound filled with fluid [103,104], while some hydrogels can enhance wound contracture to accelerate wound healing [105,106]. When a model diabetic wound was treated with FH hydrogel, the wound-healing performance was no better than the control group. This result may be because the FH hydrogel, not delivering any bioactive ingredients, failed to improve the overall

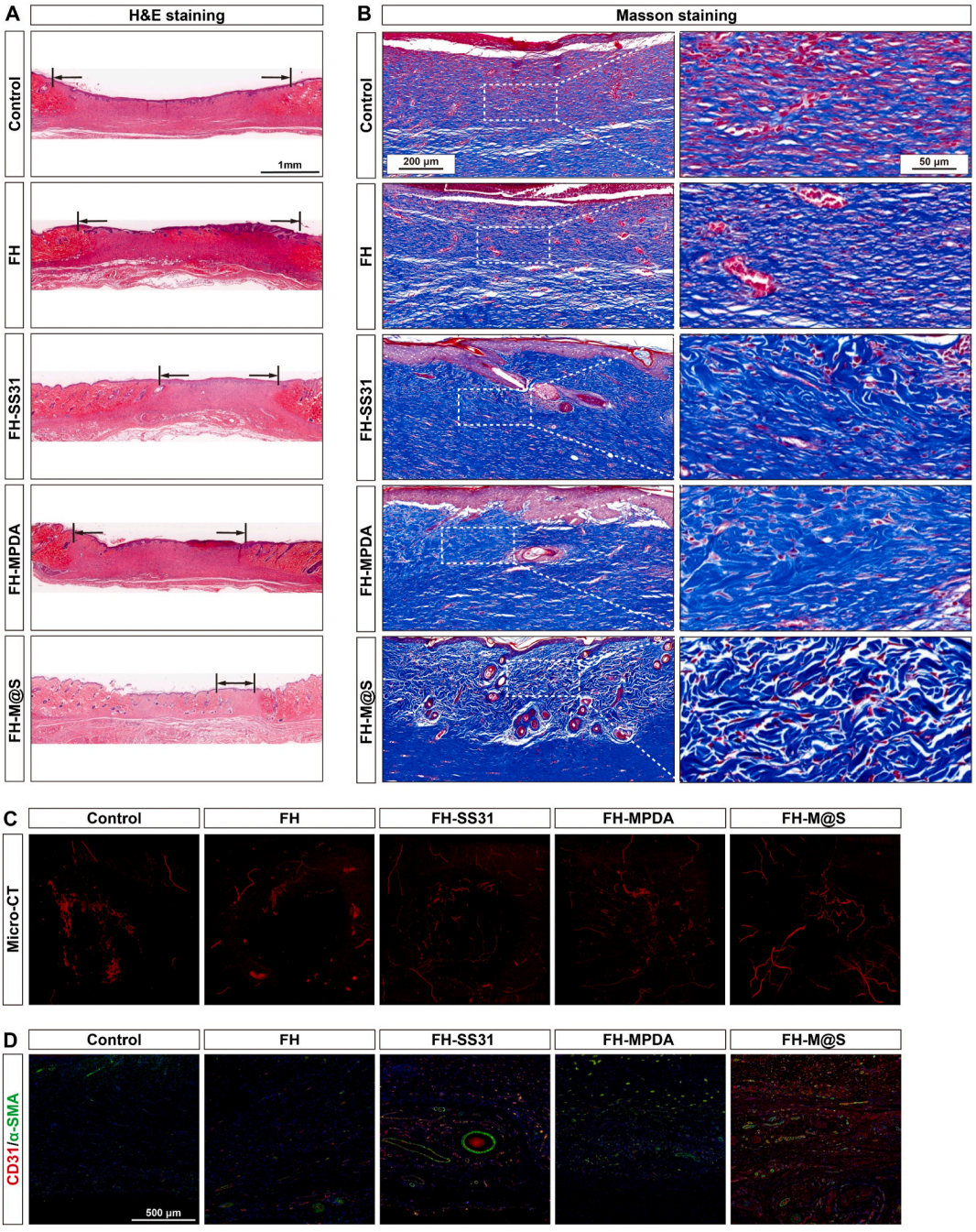

Fig. 10. Histological staining and immunofluorescence (IF) to evaluate wound healing. (A) H&E staining images of wound sections at day 14 after surgery. Scale bar, 1 mm. (B) Histological images of Masson's trichrome staining of wound sections at low and high magnification. Low magnification scale bar = 200 μm and high magnification scale bar = 50 μm. (C) 3D reconstructions of blood vessels from micro-CT at day 7 after surgery. (D) IF co-staining for α-SMA (green), CD31 (red) and DAPI (blue). Scale bar, 500 μm.

wound condition, and influenced wound contraction. In summary, compared with the control group, the FH group showed no significant difference, while the wounds treated with FH–SS31 hydrogel, FH–MPDA hydrogel, and FH–M@S hydrogel closed in remarkably shortened time and the effect of FH–M@S hydrogel was the best.

3.10. Histological staining and immunofluorescence to evaluate wound healing

Because gross morphology showed that wound healing had almost resulted in closure on day 14, in order to further evaluate wound healing, tissue samples were collected on day 14 and histological sections were observed by hematoxylin and eosin (H&E) staining and Masson's trichrome staining. The H&E staining (Fig. 10A) showed that, compared with the control group, wounds treated with FH hydrogel showed accelerated wound healing. Meanwhile in the wounds treated with the four types of hydrogels, the FH–M@S hydrogel group exhibited faster wound healing than the wounds covered with FH, FH–SS31, or FH–MPDA hydrogel. Furthermore, the wound treated with FH–M@S hydrogel appeared similar to normal skin not only in terms of re-epithelialization, but also regenerated skin appendages, which spread throughout the regenerated skin tissue. In addition, Masson's trichrome staining was used to assess the quantity and quality of collagen fibers in the wound, with blue color representing the content of collagen, and the wavy shape and oriented arrangement indicating collagen maturity [107,108]. As shown in Fig. 10B and Fig. S13, although the wounds covered with FH–SS31 hydrogel and FH–MPDA hydrogel exhibited a large amount of collagen formation, the wounds treated with FH–M@S hydrogel showed the greatest amounts and the most orderly arrangement of collagen fibers in the wound. All the results confirmed that the FH–M@S hydrogel had superior efficacy in promoting wound healing.

Vascularization plays a crucial role in wound healing, by providing sufficient nutrition and oxygen for tissue reconstruction [5,109]. We used 3D micro-CT reconstruction of the perfused blood vessels to evaluate vascular formation after 7 days of treatment. As seen in Fig. 10C, the wounds treated with FH–M@S hydrogel had the greatest volume of vessels, while the FH–SS31 hydrogel group and the FH–MPDA hydrogel group also exhibited a large amount of neovascular formation. Immunofluorescence analysis of CD31 and α-SMA was then used to evaluate the neovascularization and mature blood vessel formation at day 14. As shown in Fig. 10D and Fig. S14, the results revealed that, compared with the control group, the four hydrogel groups showed a higher degree of vessel formation. Meanwhile, among the hydrogel groups, the FH–M@S group exhibited the highest degree of vessel formation regardless of the quantity of neovasculature or vessel maturity, followed by the FH–SS31 group, the FH–MPDA group, and then the FH group. These results implied that the FH–M@S hydrogel facilitated vessel formation and then recontraction of skin tissue.

In addition to skin healing, immunoregulation is crucial to the treatment of diabetic wounds, and macrophages play an important role in the immune response [110]. Immunofluorescence analysis of CD86 (a marker of M1-like macrophages) and CD206 was used to evaluate the M1 macrophages and M2 macrophages respectively. As shown in Fig. 11A and Fig. S15, many M1 macrophages were detected in the control group and the FH group, while a few M1 macrophages were detected in the FH–SS31 group and the FH–MPDA group, and the fewest M1 macrophages were detected in the FH–M@S group. Furthermore, the FH–M@S hydrogel group exhibited the largest number of M2 macrophages, followed by the FH–SS31 hydrogel group, the FH–MPDA hydrogel group, the FH group and finally the control group. These

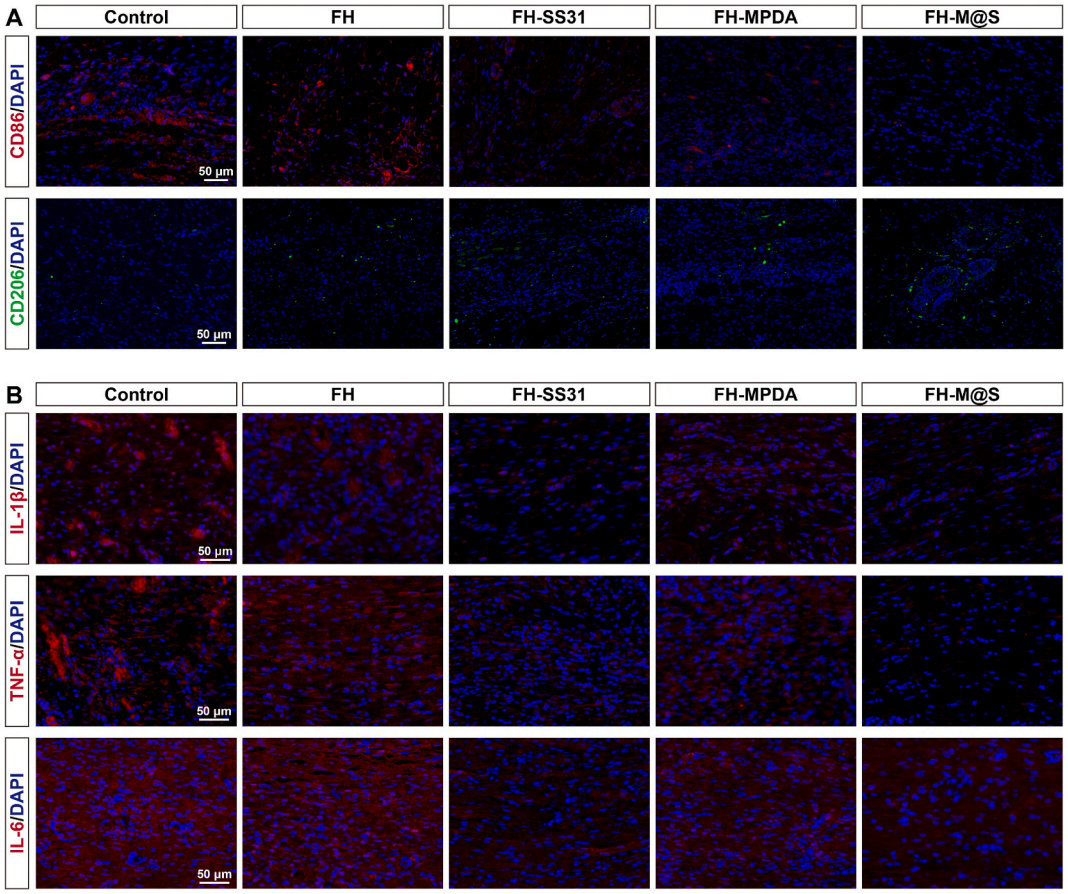

Fig. 11. IF to evaluate macrophage polarization and expression of pro-inflammatory cytokines in wound healing. (A) IF staining of CD86 (red), CD206 (green), and DAPI (blue). Scale bar, 50 μm. (B) IF staining of IL-1β (red), TNF-α (red), IL-6 (red), and DAPI (blue). Scale bar, 50 μm.

results indicated that the FH–M@S hydrogel is well able to modulate macrophage polarization. Moreover, inflammatory cytokines play a crucial role in wound healing, and we evaluated the expression of some typical pro-inflammatory cytokines *in vivo,* including IL-1β, IL-6 and TNF-α (Fig. 11B and Fig. S16). The control group exhibited the highest expression of the pro-inflammatory cytokines IL-1β, IL-6 and TNF-α, followed by the FH group, the FH–MPDA group and the FH–SS31 group, with the FH–M@S group showing the lowest expression of pro-inflammatory cytokines. These results suggested that the FH–M@S hydrogel decreased the expression of pro-inflammatory cytokines.

In the diabetic wound microenvironment, chronic hyperglycemia causes serious problems, including bacterial infection, mitochondrial dysfunction, overproduction of ROS, and microvascular dysfunction. Chronic bacterial infection increases oxidative stress and causes persistent inflammation and tissue necrosis [111]. Mitochondrial dysfunction attenuates OXPHOS and ATP production, and causes leakage of a large number of mtROS. Microvascular dysfunction reduces oxygen and nutrition delivery and hinders wound healing [112]. A mass of ROS accumulation in the wound will not only lead to endothelial dysfunction and hinder angiogenesis, but also prevent macrophages from shifting between the pro-inflammation phenotype (M1) and the anti-inflammation phenotype (M2), resulting in secretion of a lot of pro-inflammatory cytokines and persistent inflammation [113–116]. Among these problems caused by chronic hyperglycemia, the overproduction of ROS, which is primarily derived from the mitochondrial respiratory chain, plays a crucial role [9,117]. As hyperglycemia-induced mtROS increase, some biochemical pathways are activated, such as increased production of advanced glycation end products (AGEs), and activation of protein kinase C, resulting in microvascular damage and promoting M1 macrophage polarization [12,89]. Although there are various anti-oxidative treatments available, these antioxidants come with some drawbacks. For example, natural antioxidants usually need to be administered at a high dose to achieve effective concentrations because of their lack of mitochondrial targeting or hydrophobicity [14], and some enzyme-mimicking nanomaterials have shown excellent antioxidant abilities, but may cause genotoxicity or produce cytotoxic hydroxyl free radicals via peroxidase activity [112,115]. In addition, scavenging ROS indiscriminately or transforming one type of ROS to another will impact physical metabolism [6,118]. SS31 targets mitochondria, stabilizing mitochondrial function, and decreasing production of mtROS by stabilizing the ETC and reducing electron leakage [23,31], and MPDA NPs have excellent ROS-scavenging properties due to their many phenol groups [42]. The synergistic effect of MPDA NPs and SS31 can break the positive feedback loop of ROS and block inflammation.

In chronic inflammation of diabetic wounds, macrophage polarization is of great importance. M1 macrophages secrete pro-inflammatory cytokines (e.g., IL-1β, IL-6, and TNF-α) and recruit more inflammatory cells, while M2 macrophages secrete anti-inflammatory cytokines (e.g., IL-4, IL-10, and IL-13) and growth factors (e.g., EGF, TGF-β and VEGF) to accelerate wound healing [119]. In diabetic wounds, a high ROS environment impairs macrophage polarization, leading to a lot of inactivated macrophages differentiating into M1 macrophages rather than M2 macrophages [99], and resulting in chronic inflammation and non-healing wounds [120]. We treated diabetic wounds with FH–M@S hydrogel, as M@S NPs exhibited excellent anti-inflammatory and antioxidant effects, SS31 targeted mitochondria to decrease mtROS leakage, and MPDA NPs also scavenged ROS in the ECM (Figs. 7C and 8B), decreasing ROS accumulation in the diabetic wound, promoting the macrophage phenotypic switch from M1 to M2 thus restoring macrophage function (Fig. 11A), and promoting switching of the inflammatory phase to the proliferation stage [121]. In addition, in inhibiting M1 macrophage polarization and promoting M2 macrophage polarization, the performance of SS31 was better than MPDA NPs (Figs. 7D, 8D and 11A). The results of RNA-seq, after treatment with SS31, indicated activation of many inflammation-related signaling pathways. Consequently qRT-PCR and western blot assays were used to confirm the relationship between SS31 and inflammation. The results showed that SS31 increased the quantity of IκB-α, which regulates activation of the NF-κB signaling pathway [85], and inhibited the expression of pro-inflammatory cytokines, such as IL-1β and TNF-α (Fig. 6F). The results of immunofluorescence staining *in vivo* also confirmed that SS31 inhibited the expression of pro-inflammatory cytokines (Fig. 11B). In addition, FH–M@S hydrogel showed excellent photothermal properties, and it also exhibited good antibacterial properties to reduce ROS production and inflammation, after irradiation with NIR (Fig. 4B and Fig. S7). Photothermal therapy (PPT) will cause cells around the hydrogel to produce a lot of ROS and may destroy normal cells [20]. However, in contrast to other photothermal agents, the large number of phenol groups in MPDA NPs can scavenge ROS, and SS31 also targets mitochondria to reduce oxidative stress, therefore, the adverse impact of PPT can be minimized.

In the diabetic wound microenvironment, chronic hyperglycemia induces microvascular dysfunction, resulting in chronic hypoxia and ischemia [122]. Besides, many studies have suggested that microvascular destruction is attributable to overproduction of superoxide free radicals, endothelial apoptosis and chronic inflammation [96,123,124]. Previous studies indicated that SS31 was used to treat ischemic disease or ischemia–reperfusion injury such as ischemic stroke and acute kidney injury [33,125], because it prevented mitochondrial swelling, preserved cristae membranes, managed ATP production, and reduced apoptosis, necrosis and oxidative stress [13]. When diabetic wounds were treated with FH–M@S hydrogel, ROS in the wound microenvironment caused MPDA NPs to respond releasing a quantity of SS31. After SS31 activity is targeted to mitochondria, the production of mtROS will decrease via stabilization of the ETC and reduction of electron leakage [23,31], and more ATP can be used to rescue vascular formation by enhancing mitochondrial function. As a result of attenuating oxidative stress, many inflammatory signaling molecules will not activate, allowing cells to break out of the state of prolonged inflammation and enter a proliferative phase [8]. Meanwhile, strengthening oxidative stress management promotes M2 macrophage polarization, which enhances growth factor secretion to promote angiogenesis [126]. In addition, SS31 also activates the PI3K/AKT/mTOR pathway to enhance endothelial cell migration and proliferation, and thus promote angiogenesis. SS31 also reduces mitochondrial permeability transition pore opening and rejuvenates mitochondrial function, resulting in inhibition of apoptosis [127,128]. Consequently, the FH–M@S hydrogel is able to promote neovascularization and accelerate wound healing.

In summary, when a diabetic wound is treated with FH–M@S hydrogel, MPDA NPs and SS31 released from the hydrogel can exert a synergistic effect in combating bacteria, scavenging ROS, enhancing mitochondrial function, promoting cell proliferation, inhibiting apoptosis, promoting angiogenesis and ultimately promoting wound healing (Fig. 12).

3.11. Biocompatibility of FH–M@S hydrogel in vivo

The biocompatibility of FH–M@S hydrogel was assessed *in vivo*. At day 21, the major tissues including heart, spleen, liver, and kidney were collected and examined after H&E staining. As shown in Fig. S17, compared with the control group, no obvious differences were found in the hydrogel groups, indicating good biosafety of FH–M@S hydrogel *in vivo*.

The FH–M@S hydrogel dressing was considered suitable for promoting healing of diabetic cutaneous wounds. It not only meets the basic criteria for an acceptable wound dressing, adapting to wounds of various shapes and at different sites, but it also has anti-bacterial, pro-angiogenic, and inflammation-inhibiting actions and reduces oxidative stress. In addition, the biosafety of the main bioactive molecules, SS31 and MPDA NPs, is also acknowledged [13,37], and the assembly process is convenient, fast, safe, and cost effective. Hence, the FH–M@S hydrogel

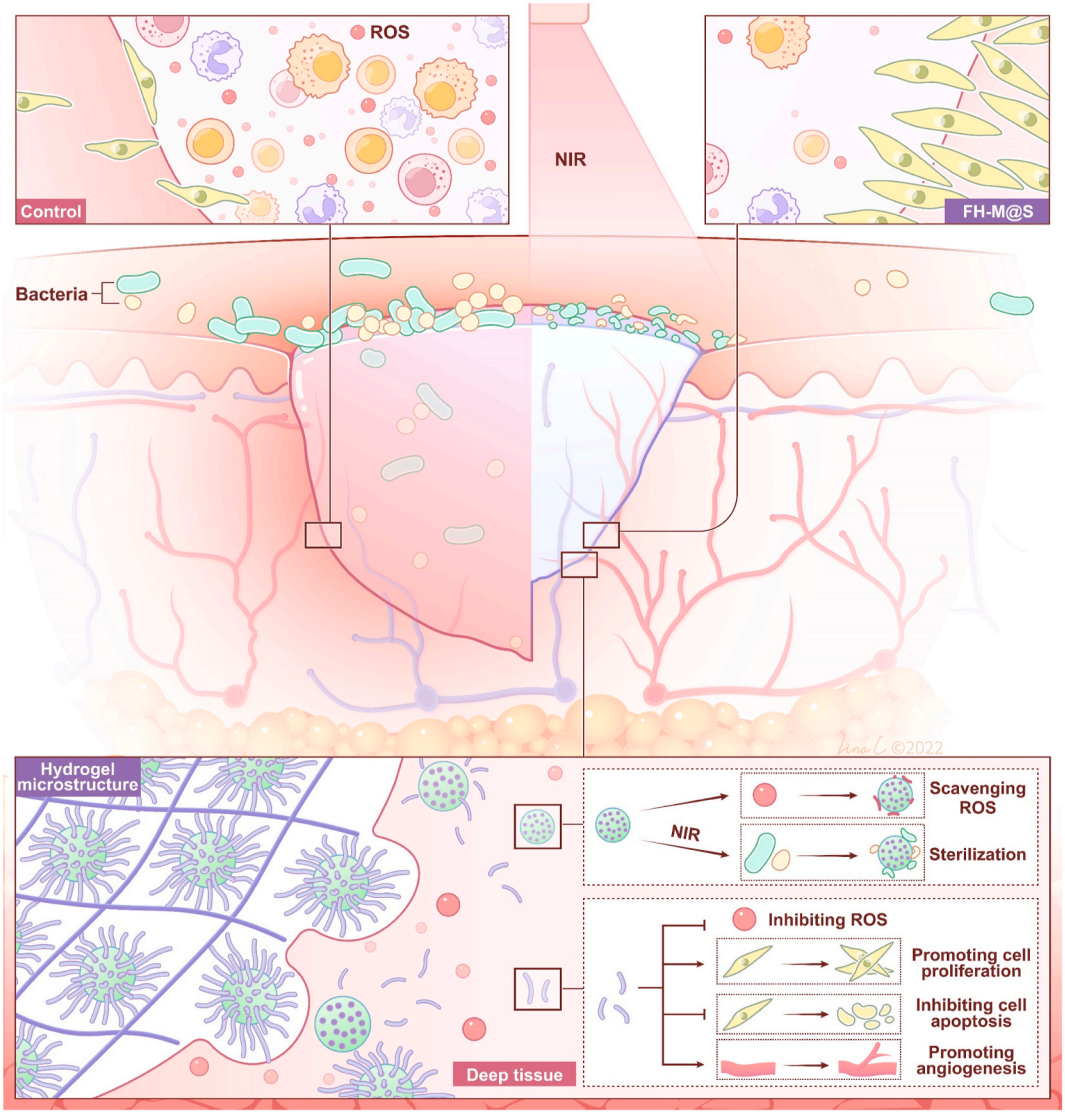

Fig. 12. Schematic illustration of FH–M@S hydrogel promoting diabetic wound healing. Illustration credit: Lina Cao.

has enormous potential in diabetic wound therapy [129].

Although we have extensively evaluated and explored FH–M@S hydrogel performance *in vitro* and *in vivo*, more research is still required to investigate the effect of SS31 in diabetic wounds. Moreover, bacterial infection plays an important role in diabetic wounds, thus a diabetic wound infection model should be established to assess the *in vivo* photothermal antibiofilm properties of FH–M@S hydrogel. In this study, we detected only small portion evidence of M@S NPs that was related to neovascularization and fibrogenesis, so more thorough and direct evidence is needed to reveal the detailed mechanism.

4. Conclusion

Altogether, we succeeded in fabricating a simple and economical FH–M@S hydrogel dressing for diabetic wound healing with sustained and ROS-responsive release of SS31. The hydrogel, as a delivery vehicle, exhibits excellent adhesion, injectability and compression and recovery properties. *In vitro*, the M@S NPs promote adhesion, migration and angiogenesis, scavenge ROS and regulate macrophage polarization, and the hydrogel can be used as a photothermal therapy agent for sterilization. The FH–M@S hydrogel dressing accelerates re-epithelialization, collagen fiber deposition and neovascularization, contributing to promoting diabetic wound closure and reconstruction of skin appendages. The mechanism is likely related to the fact that SS31 stabilizes mitochondrial function, reduces ROS production, increases ATP synthesis, inhibits inflammation, and regulates macrophage polarization. Our findings demonstrate that the FH–M@S hydrogel has great potential for diabetic wound therapy.

Ethics statement

Ethical approval was granted by the Ethics Committee of Shanghai Sixth People's Hospital Affiliated to Shanghai Jiao Tong University School of Medicine. All animal experiments were approved by the Animal Care Committee of Shanghai Sixth People's Hospital Affiliated to Shanghai Jiao Tong University School of Medicine and followed the Animal Research: Reporting of In Vivo Experiments (ARRIVE) guidelines.

Data availability

All related information in this study is available upon reasonable request.

Funding

The present study was supported by the National Natural Science Foundation of China (grant numbers 81802226, 81871834 and 82072530), the Shanghai Pujiang Program (grant number 2019PJD038), Shanghai "Rising Stars of Medical Talent" Youth Development Program (Youth Medical Talents–Specialist Program), Shanghai Jiao Tong University School of Medicine "Two–Hundred Talent" Program (grant number 2022-017), and Shanghai Sixth People's Hospital Funding (ynyq202101).

CRediT authorship contribution statement

Qing-Song Deng: Data curation, Formal analysis, Investigation, Methodology, Project administration, Validation, Visualization, Writing – original draft. **Yuan Gao:** Investigation, Methodology, Validation. **Bi-Yu Rui:** Data curation, Investigation, Methodology. **Xu-Ran Li:** Investigation, Methodology, Validation. **Po-Lin Liu:** Formal analysis. **Zi-Yin Han:** Resources. **Zhan-Ying Wei:** Resources. **Chang-Ru Zhang:** Resources. **Fei Wang:** Resources. **Helen Dawes:** Writing – review & editing. **Tong-He Zhu:** Resources. **Shi-Cong Tao:** Conceptualization, Funding acquisition, Project administration, Supervision, Writing – review & editing. **Shang-Chun Guo:** Conceptualization, Funding acquisition, Supervision.

Declaration of competing interest

The authors declare that they have no known competing financial interests or personal relationships that could have appeared to influence the work reported in this paper.

Acknowledgments

We thank the School of Materials Science and Engineering (Shanghai Jiao Tong University), Department of Materials Science (Fudan University), Analysis and testing center (Fudan University), School of Materials Science and Engineering (Tongji University), Institute of Translational Medicine (Shanghai Jiao Tong University), Shanghai Key Laboratory of Sleep Disordered Breathing, National Center for Translational Medicine (Shanghai Jiao Tong University), Shanghai Institute of Traumatology and Orthopedics, Shanghai University of Traditional Chinese Medicine, and the Animal Experimental Centre of Shanghai Sixth People's Hospital for expert assistance. We also wish to acknowledge current and previous members of our laboratories. In addition, we thank OE Biotech, Engineering for Life, Hangzhou All Peptide Biotechnology, Zhengzhou Feynman Biotechnology, and Shiyanjia Lab for providing technical support. We sincerely thank Lina Cao for schematic diagram design. Some illustrations in this work were created using BioRender.com.

Appendix A. Supplementary data

Supplementary data to this article can be found online at https://doi.org/10.1016/j.bioactmat.2023.04.004.

References

[1] L. Guo, X. Niu, X. Chen, F. Lu, J. Gao, Q. Chang, 3D direct writing egg white hydrogel promotes diabetic chronic wound healing via self-relied bioactive property, Biomaterials 282 (2022), 121406.
[2] B. Hu, M. Gao, K.O. Boakye-Yiadom, W. Ho, W. Yu, X. Xu, X.Q. Zhang, An intrinsically bioactive hydrogel with on-demand drug release behaviors for diabetic wound healing, Bioact. Mater. 6 (12) (2021) 4592–4606.
[3] D. Lou, Y. Luo, Q. Pang, W.Q. Tan, L. Ma, Gene-activated dermal equivalents to accelerate healing of diabetic chronic wounds by regulating inflammation and promoting angiogenesis, Bioact. Mater. 5 (3) (2020) 667–679.
[4] A.U.R. Khan, K. Huang, M.S. Khalaji, F. Yu, X. Xie, T. Zhu, Y. Morsi, Z. Jinzhong, X. Mo, Multifunctional bioactive core-shell electrospun membrane capable to terminate inflammatory cycle and promote angiogenesis in diabetic wound, Bioact. Mater. 6 (9) (2021) 2783–2800.
[5] Y. Li, T. Xu, Z. Tu, W. Dai, Y. Xue, C. Tang, W. Gao, C. Mao, B. Lei, C. Lin, Bioactive antibacterial silica-based nanocomposites hydrogel scaffolds with high angiogenesis for promoting diabetic wound healing and skin repair, Theranostics 10 (11) (2020) 4929–4943.
[6] H. Cho, M.R. Blatchley, E.J. Duh, S. Gerecht, Acellular and cellular approaches to improve diabetic wound healing, Adv. Drug Deliv. Rev. 146 (2019) 267–288.
[7] W. Zhu, Y. Yuan, G. Liao, L. Li, J. Liu, Y. Chen, J. Zhang, J. Cheng, Y. Lu, Mesenchymal stem cells ameliorate hyperglycemia-induced endothelial injury through modulation of mitophagy, Cell Death Dis. 9 (8) (2018) 837.
[8] T. Ma, X. Zhai, Y. Huang, M. Zhang, X. Zhao, Y. Du, C. Yan, A smart nanoplatform with photothermal antibacterial capability and antioxidant activity for chronic wound healing, Adv. Healthc Mater. 10 (13) (2021), e2100033.
[9] Z. Xu, Y. Liu, R. Ma, J. Chen, J. Qiu, S. Du, C. Li, Z. Wu, X. Yang, Z. Chen, T. Chen, Thermosensitive hydrogel incorporating Prussian blue nanoparticles promotes diabetic wound healing via ROS scavenging and mitochondrial function restoration, ACS Appl. Mater. Interfaces 14 (12) (2022) 14059–14071.
[10] S. Liu, Q. Zhang, J. Yu, N. Shao, H. Lu, J. Guo, X. Qiu, D. Zhou, Y. Huang, Absorbable thioether grafted hyaluronic acid nanofibrous hydrogel for synergistic modulation of inflammation microenvironment to accelerate chronic diabetic wound healing, Adv. Healthc Mater. 9 (11) (2020), e2000198.
[11] M. Brownlee, Biochemistry and molecular cell biology of diabetic complications, Nature 414 (6865) (2001) 813–820.
[12] S. Munusamy, L.A. MacMillan-Crow, Mitochondrial superoxide plays a crucial role in the development of mitochondrial dysfunction during high glucose exposure in rat renal proximal tubular cells, Free Radic. Biol. Med. 46 (8) (2009) 1149–1157.
[13] H.H. Szeto, A.V. Birk, Serendipity and the discovery of novel compounds that restore mitochondrial plasticity, Clin. Pharmacol. Ther. 96 (6) (2014) 672–683.
[14] M.J. Callaghan, D.J. Ceradini, G.C. Gurtner, Hyperglycemia-induced reactive oxygen species and impaired endothelial progenitor cell function, Antioxidants Redox Signal. 7 (11–12) (2005) 1476–1482.
[15] W. Cao, S. Peng, Y. Yao, J. Xie, S. Li, C. Tu, C. Gao, A nanofibrous membrane loaded with doxycycline and printed with conductive hydrogel strips promotes diabetic wound healing in vivo, Acta Biomater. 152 (2022) 60–73.
[16] Y. Yang, X. Zhao, J. Yu, X. Chen, R. Wang, M. Zhang, Q. Zhang, Y. Zhang, S. Wang, Y. Cheng, Bioactive skin-mimicking hydrogel band-aids for diabetic wound healing and infectious skin incision treatment, Bioact. Mater. 6 (11) (2021) 3962–3975.
[17] D.G. Armstrong, A.J.M. Boulton, S.A. Bus, Diabetic foot ulcers and their recurrence, N. Engl. J. Med. 376 (24) (2017) 2367–2375.
[18] B.A. Lipsky, A.R. Berendt, P.B. Cornia, J.C. Pile, E.J. Peters, D.G. Armstrong, H. G. Deery, J.M. Embil, W.S. Joseph, A.W. Karchmer, M.S. Pinzur, E. Senneville, A. Infectious Diseases Society of, 2012 Infectious Diseases Society of America clinical practice guideline for the diagnosis and treatment of diabetic foot infections, Clin. Infect. Dis. 54 (12) (2012) e132–e173.
[19] Z. Yuan, C. Lin, Y. He, B. Tao, M. Chen, J. Zhang, P. Liu, K. Cai, Near-infrared light-triggered nitric-oxide-enhanced photodynamic therapy and low-temperature photothermal therapy for biofilm elimination, ACS Nano 14 (3) (2020) 3546–3562.
[20] C. Mao, Y. Xiang, X. Liu, Y. Zheng, K.W.K. Yeung, Z. Cui, X. Yang, Z. Li, Y. Liang, S. Zhu, S. Wu, Local photothermal/photodynamic synergistic therapy by disrupting bacterial membrane to accelerate reactive oxygen species permeation and protein leakage, ACS Appl. Mater. Interfaces 11 (19) (2019) 17902–17914.
[21] C. Xuan, L. Hao, X. Liu, Y. Zhu, H. Yang, Y. Ren, L. Wang, T. Fujie, H. Wu, Y. Chen, X. Shi, C. Mao, Wet-adhesive, haemostatic and antimicrobial bilayered composite nanosheets for sealing and healing soft-tissue bleeding wounds, Biomaterials 252 (2020), 120018.
[22] J.D. Chavez, X. Tang, M.D. Campbell, G. Reyes, P.A. Kramer, R. Stuppard, A. Keller, H. Zhang, P.S. Rabinovitch, D.J. Marcinek, J.E. Bruce, Mitochondrial protein interaction landscape of SS-31, Proc. Natl. Acad. Sci. U. S. A. 117 (26) (2020) 15363–15373.
[23] H.H. Szeto, First-in-class cardiolipin-protective compound as a therapeutic agent to restore mitochondrial bioenergetics, Br. J. Pharmacol. 171 (8) (2014) 2029–2050.
[24] M.T. Sweetwyne, J.W. Pippin, D.G. Eng, K.L. Hudkins, Y.A. Chiao, M. D. Campbell, D.J. Marcinek, C.E. Alpers, H.H. Szeto, P.S. Rabinovitch, S. J. Shankland, The mitochondrial-targeted peptide, SS-31, improves glomerular architecture in mice of advanced age, Kidney Int. 91 (5) (2017) 1126–1145.
[25] A.V. Birk, S. Liu, Y. Soong, W. Mills, P. Singh, J.D. Warren, S.V. Seshan, J. D. Pardee, H.H. Szeto, The mitochondrial-targeted compound SS-31 re-energizes ischemic mitochondria by interacting with cardiolipin, J. Am. Soc. Nephrol. 24 (8) (2013) 1250–1261.
[26] D. Liu, F. Jin, G. Shu, X. Xu, J. Qi, X. Kang, H. Yu, K. Lu, S. Jiang, F. Han, J. You, Y. Du, J. Ji, Enhanced efficiency of mitochondria-targeted peptide SS-31 for acute kidney injury by pH-responsive and AKI-kidney targeted nanopolyplexes, Biomaterials 211 (2019) 57–67.
[27] G. Burnstock, G.E. Knight, A.V. Greig, Purinergic signaling in healthy and diseased skin, J. Invest. Dermatol. 132 (3 Pt 1) (2012) 526–546.
[28] J.V. Cordeiro, A. Jacinto, The role of transcription-independent damage signals in the initiation of epithelial wound healing, Nat. Rev. Mol. Cell Biol. 14 (4) (2013) 249–262.
[29] Q. Wang, H.W. Zhang, H.X. Mei, Y. Ye, H.R. Xu, S.Y. Xiang, Q. Yang, S.X. Zheng, F.G. Smith, S.W. Jin, MCTR1 enhances the resolution of lipopolysaccharide-

induced lung injury through STAT6-mediated resident M2 alveolar macrophage polarization in mice, J. Cell Mol. Med. 24 (17) (2020) 9646–9657.
[30] X. Li, R. Liu, X. Su, Y. Pan, X. Han, C. Shao, Y. Shi, Harnessing tumor-associated macrophages as aids for cancer immunotherapy, Mol. Cancer 18 (1) (2019) 177.
[31] W. Zhao, Z. Xu, J. Cao, Q. Fu, Y. Wu, X. Zhang, Y. Long, X. Zhang, Y. Yang, Y. Li, W. Mi, Elamipretide (SS-31) improves mitochondrial dysfunction, synaptic and memory impairment induced by lipopolysaccharide in mice, J. Neuroinflammation 16 (1) (2019) 230.
[32] H.H. Szeto, S. Liu, Y. Soong, N. Alam, G.T. Prusky, S.V. Seshan, Protection of mitochondria prevents high-fat diet-induced glomerulopathy and proximal tubular injury, Kidney Int. 90 (5) (2016) 997–1011.
[33] D. Liu, G. Shu, F. Jin, J. Qi, X. Xu, Y. Du, H. Yu, J. Wang, M. Sun, Y. You, M. Zhu, M. Chen, L. Zhu, Q. Shen, X. Ying, X. Lou, S. Jiang, Y. Du, ROS-responsive chitosan-SS31 prodrug for AKI therapy via rapid distribution in the kidney and long-term retention in the renal tubule, Sci. Adv. 6 (41) (2020).
[34] L. Wang, Y. He, T. He, G. Liu, C. Lin, K. Li, L. Lu, K. Cai, Lymph node-targeted immune-activation mediated by imiquimod-loaded mesoporous polydopamine based-nanocarriers, Biomaterials 255 (2020), 120208.
[35] M. Ding, Z. Miao, F. Zhang, J. Liu, X. Shuai, Z. Zha, Z. Cao, Catalytic rhodium (Rh)-based (mesoporous polydopamine) MPDA nanoparticles with enhanced phototherapeutic efficiency for overcoming tumor hypoxia, Biomater. Sci. 8 (15) (2020) 4157–4165.
[36] Y. Liu, Q. Fan, Y. Huo, C. Liu, B. Li, Y. Li, Construction of a mesoporous polydopamine@GO/cellulose nanofibril composite hydrogel with an encapsulation structure for controllable drug release and toxicity shielding, ACS Appl. Mater. Interfaces 12 (51) (2020) 57410–57420.
[37] Y. Liu, K. Ai, L. Lu, Polydopamine and its derivative materials: synthesis and promising applications in energy, environmental, and biomedical fields, Chem. Rev. 114 (9) (2014) 5057–5115.
[38] D. Wu, J. Zhou, X. Chen, Y. Chen, S. Hou, H. Qian, L. Zhang, G. Tang, Z. Chen, Y. Ping, W. Fang, H. Duan, Mesoporous polydopamine with built-in plasmonic core: traceable and NIR triggered delivery of functional proteins, Biomaterials 238 (2020), 119847.
[39] S. Xue, X. Zhou, W. Sang, C. Wang, H. Lu, Y. Xu, Y. Zhong, L. Zhu, C. He, J. Ma, Cartilage-targeting peptide-modified dual-drug delivery nanoplatform with NIR laser response for osteoarthritis therapy, Bioact. Mater. 6 (8) (2021) 2372–2389.
[40] J.W. Xu, K. Yao, Z.K. Xu, Nanomaterials with a photothermal effect for antibacterial activities: an overview, Nanoscale 11 (18) (2019) 8680–8691.
[41] Y. Fu, L. Yang, J. Zhang, J. Hu, G. Duan, X. Liu, Y. Li, Z. Gu, Polydopamine antibacterial materials, Mater. Horiz. 8 (6) (2021) 1618–1633.
[42] H. Zhao, Z. Zeng, L. Liu, J. Chen, H. Zhou, L. Huang, J. Huang, H. Xu, Y. Xu, Z. Chen, Y. Wu, W. Guo, J.H. Wang, J. Wang, Z. Liu, Polydopamine nanoparticles for the treatment of acute inflammation-induced injury, Nanoscale 10 (15) (2018) 6981–6991.
[43] D. Zheng, C. Huang, X. Zhu, H. Huang, C. Xu, Performance of polydopamine complex and mechanisms in wound healing, Int. J. Mol. Sci. 22 (19) (2021).
[44] A. Jin, Y. Wang, K. Lin, L. Jiang, Nanoparticles modified by polydopamine: working as "drug" carriers, Bioact. Mater. 5 (3) (2020) 522–541.
[45] C. Wang, M. Wang, T. Xu, X. Zhang, C. Lin, W. Gao, H. Xu, B. Lei, C. Mao, Engineering bioactive self-healing antibacterial exosomes hydrogel for promoting chronic diabetic wound healing and complete skin regeneration, Theranostics 9 (1) (2019) 65–76.
[46] Z. Tang, F. Jiang, Y. Zhang, Y. Zhang, YuanYang, X. Huang, Y. Wang, D. Zhang, N. Ni, F. Liu, M. Luo, X. Fan, W. Zhang, P. Gu, Mussel-inspired injectable hydrogel and its counterpart for actuating proliferation and neuronal differentiation of retinal progenitor cells, Biomaterials 194 (2019) 57–72.
[47] E. Jooybar, M.J. Abdekhodaie, M. Alvi, A. Mousavi, M. Karperien, P.J. Dijkstra, An injectable platelet lysate-hyaluronic acid hydrogel supports cellular activities and induces chondrogenesis of encapsulated mesenchymal stem cells, Acta Biomater. 83 (2019) 233–244.
[48] K. Fang, R. Wang, H. Zhang, L. Zhou, T. Xu, Y. Xiao, Y. Zhou, G. Gao, J. Chen, D. Liu, F. Ai, J. Fu, Mechano-responsive, tough, and antibacterial zwitterionic hydrogels with controllable drug release for wound healing applications, ACS Appl. Mater. Interfaces 12 (47) (2020) 52307–52318.
[49] Y. Wang, Y. Miao, J. Zhang, J.P. Wu, T.B. Kirk, J. Xu, D. Ma, W. Xue, Three-dimensional printing of shape memory hydrogels with internal structure for drug delivery, Mater Sci Eng C Mater Biol Appl 84 (2018) 44–51.
[50] F. Chen, Y. Xing, Z. Wang, X. Zheng, J. Zhang, K. Cai, Nanoscale polydopamine (PDA) meets pi-pi interactions: an interface-directed coassembly approach for mesoporous nanoparticles, Langmuir 32 (46) (2016) 12119–12128.
[51] M.L. Alfieri, T. Weil, D.Y.W. Ng, V. Ball, Polydopamine at biological interfaces, Adv. Colloid Interface Sci. 305 (2022), 102689.
[52] L. Ning, C. You, Y. Zhang, X. Li, F. Wang, Polydopamine loaded fluorescent nanocellulose–agarose hydrogel: a pH-responsive drug delivery carrier for cancer therapy, Compos. Commun. 26 (2021), 100739.
[53] A. Hendi, M. Umair Hassan, M. Elsherif, B. Alqattan, S. Park, A.K. Yetisen, H. Butt, Healthcare applications of pH-sensitive hydrogel-based devices: a review, Int. J. Nanomed. 15 (2020) 3887–3901.
[54] H. Pan, X. Shen, W. Tao, S. Chen, X. Ye, Fabrication of polydopamine-based curcumin nanoparticles for chemical stability and pH-responsive delivery, J. Agric. Food Chem. 68 (9) (2020) 2795–2802.
[55] S. Amorim, C.A. Reis, R.L. Reis, R.A. Pires, Extracellular matrix mimics using hyaluronan-based biomaterials, Trends Biotechnol. 39 (1) (2021) 90–104.
[56] C.C.L. Schuurmans, M. Mihajlovic, C. Hiemstra, K. Ito, W.E. Hennink, T. Vermonden, Hyaluronic acid and chondroitin sulfate (meth)acrylate-based hydrogels for tissue engineering: synthesis, characteristics and pre-clinical evaluation, Biomaterials 268 (2021), 120602.
[57] M. Nieuwdorp, F. Holleman, E. de Groot, H. Vink, J. Gort, A. Kontush, M. J. Chapman, B.A. Hutten, C.B. Brouwer, J.B. Hoekstra, J.J. Kastelein, E.S. Stroes, Perturbation of hyaluronan metabolism predisposes patients with type 1 diabetes mellitus to atherosclerosis, Diabetologia 50 (6) (2007) 1288–1293.
[58] J. Qu, X. Zhao, Y. Liang, T. Zhang, P.X. Ma, B. Guo, Antibacterial adhesive injectable hydrogels with rapid self-healing, extensibility and compressibility as wound dressing for joints skin wound healing, Biomaterials 183 (2018) 185–199.
[59] S. Li, H. Zhou, Y. Li, X. Jin, H. Liu, J. Lai, Y. Wu, W. Chen, A. Ma, Mussel-inspired self-adhesive hydrogels by conducting free radical polymerization in both aqueous phase and micelle phase and their applications in flexible sensors, J. Colloid Interface Sci. 607 (Pt 1) (2022) 431–439.
[60] P. Ren, H. Zhang, Z. Dai, F. Ren, Y. Wu, R. Hou, Y. Zhu, J. Fu, Stiff micelle-crosslinked hyaluronate hydrogels with low swelling for potential cartilage repair, J. Mater. Chem. B 7 (36) (2019) 5490–5501.
[61] X. Bai, S. Lu, Z. Cao, B. Ni, X. Wang, P. Ning, D. Ma, H. Wei, M. Liu, Dual crosslinked chondroitin sulfate injectable hydrogel formed via continuous Diels-Alder (DA) click chemistry for bone repair, Carbohydr. Polym. 166 (2017) 123–130.
[62] A.A. Barba, M. d'Amore, M. Grassi, S. Chirico, G. Lamberti, G. Titomanlio, Investigation of Pluronic© F127-Water solutions phase transitions by DSC and dielectric spectroscopy, J. Appl. Polym. Sci. 114 (2) (2009) 688–695.
[63] Y. Sun, S. Liu, G. Du, G. Gao, J. Fu, Multi-responsive and tough hydrogels based on triblock copolymer micelles as multi-functional macro-crosslinkers, Chem. Commun. 51 (40) (2015) 8512–8515.
[64] L. Teng, Z. Shao, Q. Bai, X. Zhang, Y.S. He, J. Lu, D. Zou, C. Feng, C.M. Dong, Biomimetic glycopolypeptide hydrogels with tunable adhesion and microporous structure for fast hemostasis and highly efficient wound healing, Adv. Funct. Mater. 31 (43) (2021).
[65] L. Han, K. Liu, M. Wang, K. Wang, L. Fang, H. Chen, J. Zhou, X. Lu, Mussel-Inspired adhesive and conductive hydrogel with long-lasting moisture and extreme temperature tolerance, Adv. Funct. Mater. 28 (3) (2018).
[66] K. Wei, B. Senturk, M.T. Matter, X. Wu, I.K. Herrmann, M. Rottmar, C. Toncelli, Mussel-Inspired injectable hydrogel adhesive formed under mild conditions features near-native tissue properties, ACS Appl. Mater. Interfaces 11 (51) (2019) 47707–47719.
[67] Z. Yuan, C. Lin, L. Dai, Y. He, J. Hu, K. Xu, B. Tao, P. Liu, K. Cai, Near-infrared light-activatable dual-action nanoparticle combats the established biofilms of methicillin-resistant Staphylococcus aureus and its accompanying inflammation, Small 17 (13) (2021), e2007522.
[68] M. Choi, N. Hasan, J. Cao, J. Lee, S.P. Hlaing, J.W. Yoo, Chitosan-based nitric oxide-releasing dressing for anti-biofilm and in vivo healing activities in MRSA biofilm-infected wounds, Int. J. Biol. Macromol. 142 (2020) 680–692.
[69] J. Chen, Y. Liu, G. Cheng, J. Guo, S. Du, J. Qiu, C. Wang, C. Li, X. Yang, T. Chen, Z. Chen, Tailored hydrogel delivering niobium carbide boosts ROS-scavenging and antimicrobial activities for diabetic wound healing, Small 18 (27) (2022), e2201300.
[70] H. Zhao, J. Huang, Y. Li, X. Lv, H. Zhou, H. Wang, Y. Xu, C. Wang, J. Wang, Z. Liu, ROS-scavenging hydrogel to promote healing of bacteria infected diabetic wounds, Biomaterials 258 (2020), 120286.
[71] Y. Long, L. Li, T. Xu, X. Wu, Y. Gao, J. Huang, C. He, T. Ma, L. Ma, C. Cheng, C. Zhao, Hedgehog artificial macrophage with atomic-catalytic centers to combat Drug-resistant bacteria, Nat. Commun. 12 (1) (2021) 6143.
[72] Z. Yuan, B. Tao, Y. He, C. Mu, G. Liu, J. Zhang, Q. Liao, P. Liu, K. Cai, Remote eradication of biofilm on titanium implant via near-infrared light triggered photothermal/photodynamic therapy strategy, Biomaterials 223 (2019), 119479.
[73] M.M. Cowan, Plant products as antimicrobial agents, Clin. Microbiol. Rev. 12 (4) (1999) 564–582.
[74] G. Gao, Y.W. Jiang, W. Sun, Y. Guo, H.R. Jia, X.W. Yu, G.Y. Pan, F.G. Wu, Molecular targeting-mediated mild-temperature photothermal therapy with a smart albumin-based nanodrug, Small 15 (33) (2019), e1900501.
[75] X. Dong, J. Ye, Y. Chen, T. Tanziela, H. Jiang, X. Wang, Intelligent peptide-nanorods against drug-resistant bacterial infection and promote wound healing by mild-temperature photothermal therapy, Chem. Eng. J. 432 (2022).
[76] S. Du, H. Suo, G. Xie, Q. Lyu, M. Mo, Z. Xie, N. Zhou, L. Zhang, J. Tao, J. Zhu, Self-powered and photothermal electronic skin patches for accelerating wound healing, Nano Energy 93 (2022).
[77] X. Yi, Q.Y. Duan, F.G. Wu, Low-temperature photothermal therapy: strategies and applications, Research 2021 (2021), 9816594.
[78] Y. He, J. Leng, K. Li, K. Xu, C. Lin, Z. Yuan, R. Zhang, D. Wang, B. Tao, T.J. Huang, K. Cai, A multifunctional hydrogel coating to direct fibroblast activation and infected wound healing via simultaneously controllable photobiomodulation and photodynamic therapies, Biomaterials 278 (2021), 121164.
[79] A.V. Corazza, J. Jorge, C. Kurachi, V.S. Bagnato, Photobiomodulation on the angiogenesis of skin wounds in rats using different light sources, Photomed Laser Surg 25 (2) (2007) 102–106.
[80] E.J. Lesnefsky, T.I. Gudz, S. Moghaddas, C.T. Migita, M. Ikeda-Saito, P.J. Turkaly, C.L. Hoppel, Aging decreases electron transport complex III activity in heart interfibrillar mitochondria by alteration of the cytochrome c binding site, J. Mol. Cell. Cardiol. 33 (1) (2001) 37–47.
[81] X. Xi, J. Wang, Y. Qin, Y. You, W. Huang, J. Zhan, The biphasic effect of flavonoids on oxidative stress and cell proliferation in breast cancer cells, Antioxidants 11 (4) (2022).

[82] M. Xu, J. Du, J. Cui, S. Zhang, S. Zhang, M. Deng, W. Zhang, H. Li, Z. Yu, Cell-free fat extract prevents tail suspension-induced bone loss by inhibiting osteocyte apoptosis, Front. Bioeng. Biotechnol. 10 (2022), 818572.
[83] H. Zhang, N.N. Alder, W. Wang, H. Szeto, D.J. Marcinek, P.S. Rabinovitch, Reduction of elevated proton leak rejuvenates mitochondria in the aged cardiomyocyte, Elife 9 (2020).
[84] X. Kuang, S. Zhou, W. Guo, Z. Wang, Y. Sun, H. Liu, SS-31 peptide enables mitochondrial targeting drug delivery: a promising therapeutic alteration to prevent hair cell damage from aminoglycosides, Drug Deliv. 24 (1) (2017) 1750–1761.
[85] T. Liu, L. Zhang, D. Joo, S.C. Sun, NF-kappaB signaling in inflammation, Signal Transduct. Targeted Ther. 2 (2017), 17023.
[86] Q. Tang, T. Lim, X.J. Wei, Q.Y. Wang, J.C. Xu, L.Y. Shen, Z.Z. Zhu, C.Q. Zhang, A free-standing multilayer film as a novel delivery carrier of platelet lysates for potential wound-dressing applications, Biomaterials 255 (2020), 120138.
[87] S.C. Tao, X.R. Li, W.J. Wei, Z.Y. Wei, C.R. Zhang, F. Wang, H. Dawes, S.C. Guo, Polymeric coating on beta-TCP scaffolds provides immobilization of small extracellular vesicles with surface-functionalization and ZEB1-Loading for bone defect repair in diabetes mellitus, Biomaterials 283 (2022), 121465.
[88] Y. Duan, H. Zheng, Z. Li, Y. Yao, J. Ding, X. Wang, J.R. Nakkala, D. Zhang, Z. Wang, X. Zuo, X. Zheng, J. Ling, C. Gao, Unsaturated polyurethane films grafted with enantiomeric polylysine promotes macrophage polarization to a M2 phenotype through PI3K/Akt1/mTOR axis, Biomaterials 246 (2020), 120012.
[89] Y. Sun, B. Bao, Y. Zhu, J. Shen, X. Liu, T. Gao, J. Lin, T. Huang, J. Xu, Y. Chai, X. Zheng, An FPS-ZM1-encapsulated zeolitic imidazolate framework as a dual proangiogenic drug delivery system for diabetic wound healing, Nano Res. 15 (6) (2022) 5216–5229.
[90] H. Jin, J. Seo, S.Y. Eun, Y.N. Joo, S.W. Park, J.H. Lee, K.C. Chang, H.J. Kim, P2Y2 R activation by nucleotides promotes skin wound-healing process, Exp. Dermatol. 23 (7) (2014) 480–485.
[91] G.R. Ehring, I.L. Szabó, M.K. Jones, I.J. Sarfeh, A.S. Tarnawski, ATP-induced CA2 +-signaling enhances rat gastric microvascular endothelial cell migration, J. Physiol. Pharmacol. 51 (4 Pt 2) (2000) 799–811.
[92] S. Cheng, D. Wang, J. Ke, L. Ma, J. Zhou, H. Shao, H. Zhu, L. Liu, Y. Zhang, F. Peng, X. Liu, Improved in vitro angiogenic behavior of human umbilical vein endothelial cells with oxidized polydopamine coating, Colloids Surf. B Biointerfaces 194 (2020), 111176.
[93] S. Zhong, R. Luo, X. Wang, L. Tang, J. Wu, J. Wang, R. Huang, H. Sun, N. Huang, Effects of polydopamine functionalized titanium dioxide nanotubes on endothelial cell and smooth muscle cell, Colloids Surf. B Biointerfaces 116 (2014) 553–560.
[94] T. Zhou, L. Yan, C. Xie, P. Li, L. Jiang, J. Fang, C. Zhao, F. Ren, K. Wang, Y. Wang, H. Zhang, T. Guo, X. Lu, A mussel-inspired persistent ROS-scavenging, electroactive, and osteoinductive scaffold based on electrochemical-driven in situ nanoassembly, Small 15 (25) (2019), e1805440.
[95] S. Matoori, A. Veves, D.J. Mooney, Advanced bandages for diabetic wound healing, Sci. Transl. Med. 13 (585) (2021).
[96] M. Chang, T.T. Nguyen, Strategy for treatment of infected diabetic foot ulcers, Acc. Chem. Res. 54 (5) (2021) 1080–1093.
[97] W. Zhou, Z. Duan, J. Zhao, R. Fu, C. Zhu, D. Fan, Glucose and MMP-9 dual-responsive hydrogel with temperature sensitive self-adaptive shape and controlled drug release accelerates diabetic wound healing, Bioact. Mater. 17 (2022) 1–17.
[98] F. Tang, J. Li, W. Xie, Y. Mo, L. Ouyang, F. Zhao, X. Fu, X. Chen, Bioactive glass promotes the barrier functional behaviors of keratinocytes and improves the Re-epithelialization in wound healing in diabetic rats, Bioact. Mater. 6 (10) (2021) 3496–3506.
[99] Y. Lu, H. Li, J. Wang, M. Yao, Y. Peng, T. Liu, Z. Li, G. Luo, J. Deng, Engineering bacteria-activated multifunctionalized hydrogel for promoting diabetic wound healing, Adv. Funct. Mater. 31 (48) (2021).
[100] D. Gao, Y. Zhang, D.T. Bowers, W. Liu, M. Ma, Functional hydrogels for diabetic wound management, APL Bioengineering 5 (3) (2021).
[101] Z. Pan, H. Ye, D. Wu, Recent advances on polymeric hydrogels as wound dressings, APL Bioeng 5 (1) (2021), 011504.
[102] Y. Liang, J. He, B. Guo, Functional hydrogels as wound dressing to enhance wound healing, ACS Nano 15 (8) (2021) 12687–12722.
[103] X. Peng, Y. Li, T. Li, Y. Li, Y. Deng, X. Xie, Y. Wang, G. Li, L. Bian, Coacervate-derived hydrogel with effective water repulsion and robust underwater bioadhesion promotes wound healing, Adv. Sci. 9 (31) (2022), e2203890.
[104] D.R. Griffin, M.M. Archang, C.H. Kuan, W.M. Weaver, J.S. Weinstein, A.C. Feng, A. Ruccia, E. Sideris, V. Ragkousis, J. Koh, M.V. Plikus, D. Di Carlo, T. Segura, P. O. Scumpia, Activating an adaptive immune response from a hydrogel scaffold imparts regenerative wound healing, Nat. Mater. 20 (4) (2021) 560–569.
[105] J. Hu, T. Wei, H. Zhao, M. Chen, Y. Tan, Z. Ji, Q. Jin, J. Shen, Y. Han, N. Yang, L. Chen, Z. Xiao, H. Zhang, Z. Liu, Q. Chen, Mechanically active adhesive and immune regulative dressings for wound closure, Matter 4 (9) (2021) 2985–3000.
[106] J. Wu, S. Yao, H. Zhang, W. Man, Z. Bai, F. Zhang, X. Wang, D. Fang, Y. Zhang, Liquid crystal elastomer metamaterials with giant biaxial thermal shrinkage for enhancing skin regeneration, Adv. Mater. 33 (45) (2021), e2106175.
[107] X. Zhang, Y. Li, Z. Ma, D. He, H. Li, Modulating degradation of sodium alginate/bioglass hydrogel for improving tissue infiltration and promoting wound healing, Bioact. Mater. 6 (11) (2021) 3692–3704.
[108] R. Chen, C. Zhao, Z. Chen, X. Shi, H. Zhu, Q. Bu, L. Wang, C. Wang, H. He, A bionic cellulose nanofiber-based nanocage wound dressing for NIR-triggered multiple synergistic therapy of tumors and infected wounds, Biomaterials 281 (2022), 121330.
[109] Q. Yao, Q.H. Lan, X. Jiang, C.C. Du, Y.Y. Zhai, X. Shen, H.L. Xu, J. Xiao, L. Kou, Y. Z. Zhao, Bioinspired biliverdin/silk fibroin hydrogel for antiglioma photothermal therapy and wound healing, Theranostics 10 (25) (2020) 11719–11736.
[110] H. Lei, D. Fan, A combination therapy using electrical stimulation and adaptive, conductive hydrogels loaded with self-assembled nanogels incorporating short interfering RNA promotes the repair of diabetic chronic wounds, Adv. Sci. (2022), e2201425.
[111] P. Wu, D. Chen, H. Yang, C. Lai, C. Xuan, Y. Chen, X. Shi, Antibacterial peptide-modified collagen nanosheet for infected wound repair, Smart Materials in Medicine 2 (2021) 172–181.
[112] Y. Li, R. Fu, Z. Duan, C. Zhu, D. Fan, Artificial nonenzymatic antioxidant MXene nanosheet-anchored injectable hydrogel as a mild photothermal-controlled oxygen release platform for diabetic wound healing, ACS Nano 16 (5) (2022) 7486–7502.
[113] H. Li, X. Liang, Y. Chen, K. Liu, X. Fu, C. Zhang, X. Wang, J. Yang, Synergy of Antioxidant and M2 Polarization in Polyphenol-modified Konjac Glucomannan Dressing for Remodeling Wound Healing Microenvironment, Bioengineering & Translational Medicine, 2022.
[114] L. Wang, B. Zhu, Y. Deng, T. Li, Q. Tian, Z. Yuan, L. Ma, C. Cheng, Q. Guo, L. Qiu, Biocatalytic and antioxidant nanostructures for ROS scavenging and biotherapeutics, Adv. Funct. Mater. 31 (31) (2021).
[115] L. Li, S. Cao, Z. Wu, R. Guo, L. Xie, L. Wang, Y. Tang, Q. Li, X. Luo, L. Ma, C. Cheng, L. Qiu, Modulating electron transfer in vanadium-based artificial enzymes for enhanced ROS-catalysis and disinfection, Adv. Mater. 34 (17) (2022), e2108646.
[116] Y. Dong, Y. Zheng, K. Zhang, Y. Yao, L. Wang, X. Li, J. Yu, B. Ding, Electrospun nanofibrous materials for wound healing, Advanced Fiber Materials 2 (4) (2020) 212–227.
[117] K. Green, M.D. Brand, M.P. Murphy, Prevention of mitochondrial oxidative damage as a therapeutic strategy in diabetes, Diabetes 53 (Suppl 1) (2004) S110–S118.
[118] T. Kurahashi, J. Fujii, Roles of antioxidative enzymes in wound healing, J. Dev. Biol. 3 (2) (2015) 57–70.
[119] M. Tian, L. Zhou, C. Fan, L. Wang, X. Lin, Y. Wen, L. Su, H. Dong, Bimetal-organic framework/GOx-based hydrogel dressings with antibacterial and inflammatory modulation for wound healing, Acta Biomater. 158 (2023) 252–265.
[120] C. Tu, H. Lu, T. Zhou, W. Zhang, L. Deng, W. Cao, Z. Yang, Z. Wang, X. Wu, J. Ding, F. Xu, C. Gao, Promoting the healing of infected diabetic wound by an anti-bacterial and nano-enzyme-containing hydrogel with inflammation-suppressing, ROS-scavenging, oxygen and nitric oxide-generating properties, Biomaterials 286 (2022), 121597.
[121] Z. Chen, L. Wang, C. Guo, M. Qiu, L. Cheng, K. Chen, J. Qi, L. Deng, C. He, X. Li, Y. Yan, Vascularized polypeptide hydrogel modulates macrophage polarization for wound healing, Acta Biomater. 155 (2023) 218–234.
[122] X. Zhao, D. Pei, Y. Yang, K. Xu, J. Yu, Y. Zhang, Q. Zhang, G. He, Y. Zhang, A. Li, Y. Cheng, X. Chen, Green tea derivative driven smart hydrogels with desired functions for chronic diabetic wound treatment, Adv. Funct. Mater. 31 (18) (2021).
[123] K.N.S. Rao, X. Shen, S. Pardue, D.M. Krzywanski, Nicotinamide nucleotide transhydrogenase (NNT) regulates mitochondrial ROS and endothelial dysfunction in response to angiotensin II, Redox Biol. 36 (2020), 101650.
[124] C. Jing, G. Zhang, Z. Liu, Q. Xu, C. Li, G. Cheng, R. Shi, Peroxidasin promotes diabetic vascular endothelial dysfunction induced by advanced glycation end products via NOX2/HOCl/Akt/eNOS pathway, Redox Biol. 45 (2021), 102031.
[125] C.X. Zhang, Y. Cheng, D.Z. Liu, M. Liu, H. Cui, B.L. Zhang, Q.B. Mei, S.Y. Zhou, Mitochondria-targeted cyclosporin A delivery system to treat myocardial ischemia reperfusion injury of rats, J. Nanobiotechnol. 17 (1) (2019) 18.
[126] P. Wu, Y. Liang, G. Sun, Engineering immune-responsive biomaterials for skin regeneration, Biomater Transl 2 (1) (2021) 61–71.
[127] H.N. Sabbah, R.C. Gupta, S. Kohli, M. Wang, S. Hachem, K. Zhang, Chronic therapy with elamipretide (MTP-131), a novel mitochondria-targeting peptide, improves left ventricular and mitochondrial function in dogs with advanced heart failure, Circ Heart Fail 9 (2) (2016), e002206.
[128] D.F. Dai, T. Chen, H. Szeto, M. Nieves-Cintron, V. Kutyavin, L.F. Santana, P. S. Rabinovitch, Mitochondrial targeted antioxidant Peptide ameliorates hypertensive cardiomyopathy, J. Am. Coll. Cardiol. 58 (1) (2011) 73–82.
[129] Q. Tang, T. Lim, L.Y. Shen, G. Zheng, X.J. Wei, C.Q. Zhang, Z.Z. Zhu, Well-dispersed platelet lysate entrapped nanoparticles incorporate with injectable PDLLA-PEG-PDLLA triblock for preferable cartilage engineering application, Biomaterials 268 (2021), 120605.